# A Stochastic Framework for Real-Time Quantum Field Dynamics

Xiao Lin*
Independent Researcher, Beijing 100000, China

2026-06-29

**Abstract**

We propose a Stochastic Formulation that establishes a direct mathematical correspondence between the real-time Feynman path integral in Minkowski spacetime and the expectation values of classical stochastic processes. This framework offers an alternative approach to quantum dynamics by formulating evolution through intrinsic stochastic processes rather than relying solely on pre-discretized spacetime backgrounds. Specifically, we demonstrate that the unitary dynamics of scalar fields can be mapped to continuous Wiener processes or Ornstein-Uhlenbeck process, while spinor fields correspond to discrete Poisson jump processes. Distinct from conventional methods involving perturbative expansions, Euclideanization, or Grassmann algebra, our formulation provides a non-perturbative, real-time framework where quantum amplitudes are derived statistically from stochastic trajectories.

We implement this framework via a tree-grid recursion scheme or Monte Carlo method for the Klein-Gordon field, benchmarked against exact solutions of the forced harmonic oscillator. For the Dirac field, we derive an analytical closed-form finite difference scheme that effectively models its evolution. By integrating these schemes, we successfully apply the framework to the Yukawa coupling model and extend it to QED. The results reveal non-trivial dynamical features, such as the independence of dynamical mass generation from the initial fermion mass. Crucially, the structural nature of this stochastic approach inherently avoids the fermion doubling and sign problems often encountered in lattice approaches. The extension to non-Abelian gauge theories, including SU(2) Yang-Mills and SU(3) QCD, demonstrates dynamical fermion mass generation in the chiral limit, driven purely by gauge field self-interactions, with results consistent with chiral symmetry breaking and lattice QCD calculations.

**Key words:** Quantum Field Theory, Feynman Path Integral, Stochastic Analysis, Wiener Process, Ornstein-Uhlenbeck process, Poisson Process.

*Email: xiao_lin_99@yahoo.com

# 1 Introduction

The Feynman path integral has provided quantum field theory (QFT) with a profound functional formulation based on the principle of least action. While conceptually elegant, its direct implementation in real-time Minkowski spacetime presents significant technical challenges due to the oscillatory nature of the integrand. To address these challenges, the community has developed powerful established frameworks, primarily perturbative expansions and lattice discretizations.

Perturbative methods, employing Feynman diagram techniques, have achieved remarkable success in weakly coupled regimes [1]. They serve as the cornerstone for precision calculations in the Standard Model. However, in order to fully explore the non-perturbative regime—essential for understanding phenomena such as dynamical mass generation—methods beyond the perturbation series are required.

Lattice field theory offers a robust non-perturbative alternative by discretizing spacetime, often utilizing a Euclidean formulation to map the path integral to a statistical partition function [2]. This approach has been highly successful in determining static properties of Quantum Chromodynamics (QCD). Nevertheless, the investigation of real-time dynamics and systems at finite density remains a frontier where standard Euclidean lattice techniques face inherent limitations. Specifically, the analytic continuation from Euclidean time is ill-posed for non-equilibrium processes, and the simulation of fermions in these regimes is computationally demanding due to the complex phase of the determinant. Consequently, there is a strong motivation to develop complementary approaches that operate directly within the Minkowski framework to investigate these deeper dynamical questions.

Other analytic approaches, such as instanton configurations or Schwinger-Dyson equations, provide valuable insights but often rely on specific approximations or truncations. Therefore, a direct numerical or analytic framework capable of handling time-dependent, strongly coupled systems in real time would provide a valuable addition to the existing theoretical toolkit.

We propose that these challenges can be addressed by revisiting the mathematical foundation of the path integral, specifically by relaxing the requirement for a rigid, pre-discretized

spacetime background. In this work, we introduce a stochastic framework that decouples quantum evolution from fixed spatial coordinates. Instead of treating space and time as a fundamental stage, we formulate dynamics as an *intrinsic stochastic process*, where physical observables emerge statistically from random trajectories. Specifically, we map scalar fields to continuous Wiener processes (or Ornstein-Uhlenbeck processes) and spinor fields to discrete Poisson jump processes. This stochastic formulation operates without explicit spatial discretization or Grassmann variables. In this picture, particle "position" is derived as a statistical outcome of the stochastic flow rather than a primary grid variable. By establishing a structural isomorphism between the Minkowski path integral and classical stochastic expectations, we provide a direct, real-time framework for studying strongly coupled systems, naturally circumventing the constraints associated with Euclideanization and lattice artifacts.

The structure of this paper is as follows: Sections 2 and 3 detail the Wiener/Ornstein-Uhlenbeck process formulation for the Klein-Gordon field, establishing a recursion scheme and Monte Carlo method, and validating its accuracy against exact solutions of the forced harmonic oscillator. Sections 4 and 5 construct the Poisson jump process formulation for the free Dirac spinor field, providing a stochastic bosonization of fermionic dynamics that inherently avoids the use of Grassmann algebra. Section 6 applies the full framework to the Yukawa coupling model, calculating the time-dependent evolution of the fermion effective mass and comparing the results with one-loop perturbation theory to illustrate non-perturbative dynamical effects. Section 7 extends this approach to Quantum Electrodynamics (QED), illustrating the framework's capability to handle gauge interactions and real-time photon-fermion dynamics, offering an alternative perspective to standard lattice formulations. Section 8 generalizes the framework to non-Abelian gauge theories by formulating SU(2) Yang-Mills theory coupled to a Dirac fermion, demonstrating dynamical mass generation in the chiral limit. Section 9 further extends the formalism to SU(3) Yang-Mills theory (QCD) with quarks, showing that the observed mass shift is consistent with chiral symmetry breaking and lattice QCD results. Relevant analytic derivations are provided in the Appendices.

## 2 Stochastic formulation of the scalar field

Let $\phi(x)$ be a real massive Klein–Gordon scalar field, where $x = (t, \vec{x})$ denotes spacetime coordinates. Consider the coupling of the scalar field $\phi(x)$ to an external source $\hat{J}(x)$. The Lagrangian density of the system is

$$\mathcal{L}(\phi, \partial_\mu\phi, \hat{J}) = \frac{1}{2}(\partial_t\phi)^2 - \frac{1}{2}(\nabla\phi)^2 - \frac{1}{2}m^2\phi^2 + \hat{J}(x)\phi(x). \tag{2.1}$$

According to quantum field theory, the transition amplitude from an initial state $|\phi_0, t_0\rangle$ to a final state $|\phi_T, T\rangle$ can be expressed as the following Feynman path integral:

$$\langle\phi_T, T \,|\, \phi_0, t_0\rangle = \int \mathcal{D}\phi \, \exp\big[\mathrm{i}S\big] =: K(\phi_T, T; \phi_0, t_0), \tag{2.2}$$

where the action $S$ is given by

$$S = \int \mathrm{d}^4x \, \mathcal{L}(\phi, \partial_\mu\phi, \hat{J}). \tag{2.3}$$

Here $\phi_0 = \phi(t_0, \vec{x}_0)$, $\phi_T = \phi(T, \vec{x})$, and the integration measure $\mathrm{d}^4x = \mathrm{d}t\,\mathrm{d}^3x$ integrates $t$ from $t_0$ to $T$ and $\vec{x}$ over all space.

The physical interpretation of Eq. (2.2) is that the amplitude for the field variable $\phi$ to propagate from $(t_0, \vec{x}_0)$ to $(t, \vec{x})$ equals a weighted superposition of all possible field configurations $\mathcal{D}\phi$ between these two points, with the weight determined by the phase factor $\exp(\mathrm{i}S)$. This interpretation suggests that when the external source $\hat{J}$ is too complicated to allow an analytic solution for $\phi(x)$, one may attempt to obtain the transition amplitude by numerically simulating the possible paths of the field $\phi(x)$.

This paper focuses on the scenario where the field undergoes a localized excitation in space within a very short time interval, such as during an instantaneous high-energy collision in a particle accelerator. The long-term and large-scale evolution of the quantum field can be regarded as a superposition of numerous such localized excitations. To handle this situation, we attempt to introduce new degrees of freedom into the state function $\phi(t, \vec{x})$ to replace its dependence on the spatial coordinate $\vec{x}$. We therefore assume that the spatial variation of $\phi$ is concentrated near the origin, expressing $\phi(x)$ as a product of a function of $t$ and a spherically symmetric exponential function of $\vec{x}$:

$$\phi(t, \vec{x}) = \sqrt{\frac{\kappa^3}{\pi}} e^{-\kappa r}\varphi(t), \quad r = |\vec{x}|. \tag{2.4}$$

Thus,

$$(\partial_t\phi)^2 = \frac{\kappa^3}{\pi}e^{-2\kappa r}\dot{\varphi}^2(t), \qquad (\nabla\phi)^2 = \kappa^2\cdot\frac{\kappa^3}{\pi}e^{-2\kappa r}\varphi^2(t).$$

We then Substitute these into Eq. (2.3) and perform the spatial integration in spherical coordinates. Since

$$\begin{aligned}
\int \mathrm{d}^3x\,(\partial_t\phi)^2 &= 4\pi\int r^2\mathrm{d}r\,\frac{\kappa^3}{\pi}e^{-2\kappa r}\dot{\varphi}^2(t) = \dot{\varphi}^2(t),\\
\int \mathrm{d}^3x\,(\nabla\phi)^2 &= 4\pi\int r^2\mathrm{d}r\,\frac{\kappa^5}{\pi}e^{-2\kappa r}\dot{\varphi}^2(t) = \kappa^2\varphi^2(t),\\
\int \mathrm{d}^3x\,\hat{J}(x)\phi(x) &= J(t)\varphi(t).
\end{aligned}$$

The total action then becomes:

$$S = \int_{t_0}^{T}\mathrm{d}t\left[\frac{1}{2}\dot{\varphi}^2(t) - \frac{1}{2}\omega^2\varphi^2(t) + J\varphi\right], \tag{2.5}$$

where $\omega = \sqrt{\kappa^2+m^2}$. The constant $\kappa$, which arises from the relativistic energy-momentum relation, represents the increase in effective mass due to high-energy states and can be determined experimentally based on collision velocities. Thus, we obtain the Feynman path integral formula for the transition amplitude of a free scalar field under a localized excitation driven by an external source $J$:

$$K = \int\mathcal{D}\varphi\exp\left\{\mathrm{i}\int_{t_0}^{T}\mathrm{d}t\left[\frac{1}{2}\dot{\varphi}^2(t) - \frac{1}{2}\omega^2\varphi^2(t) + J\varphi\right]\right\}. \tag{2.6}$$

To obtain the path distribution for the evolution of $\varphi$, we follow Feynman's approach [5] by discretizing the time interval $[t_0, T]$ into $N$ equal segments of length $\Delta t = (T-t_0)/N$. Denote the $n$-th time point as $t^n = t_0 + n\Delta t$, and let $\varphi^n$ represent the value of $\varphi(t)$ in the interval $[t^n, t^{n+1})$. The action $S$ can then be expressed as:

$$S = \sum_{n=0}^{N-1}\Delta t\Big[\frac{1}{2}\Big(\frac{\varphi^{n+1}-\varphi^n}{\Delta t}\Big)^2 - \frac{1}{2}\omega^2(\varphi^n)^2 + J\varphi^n\Big], \tag{2.7}$$

and the integration measure becomes:

$$\mathcal{D}\varphi = \frac{1}{\sqrt{2\pi\Delta t\,\mathrm{i}}}\prod_{n=1}^{N-1}\left[\int_{-\infty}^{\infty}\frac{\mathrm{d}\varphi^n}{\sqrt{2\pi\Delta t\,\mathrm{i}}}\right]. \tag{2.8}$$

The number of $\mathrm{d}\varphi^n$ is one less than the number of intervals $N$, because the initial point $\varphi^0$ and final point $\varphi^N$ are fixed; the path integral is only defined over the $N-1$ intermediate time points $t^1, t^2, \ldots, t^{N-1}$. However, for notational uniformity and analytical convenience, we treat the endpoint $\varphi^N$ as a variable by adding an extra integration measure $\mathrm{d}\varphi^N/\sqrt{2\pi\Delta t\,\mathrm{i}}$. In numerical computations, specific values at desired points can be extracted accordingly. The initial point $\varphi^0$ is formally assigned a measure $\mathrm{d}\varphi^0 = \delta(\varphi^0 - \varphi(t_0))$, and the prefactor in $\mathcal{D}\varphi$ is absorbed into the product; special handling is applied during numerical implementation. Consequently, the transition amplitude can be written as:

$$\begin{aligned} K &= \prod_{n=0}^{N}\left[\int_{-\infty}^{\infty}\frac{\mathrm{d}\varphi^n}{\sqrt{2\pi\Delta t\,\mathrm{i}}}\right]\cdot\prod_{n=0}^{N}\left[\exp\left(\mathrm{i}\frac{(\varphi^{n+1}-\varphi^n)^2}{2\Delta t}-\frac{\mathrm{i}\Delta t}{2}\omega^2(\varphi^n)^2+\mathrm{i}\Delta t J\varphi^n\right)\right] \\ &= \prod_{n=0}^{N}\left\{\int_{-\infty}^{\infty}\frac{\mathrm{d}\varphi^n}{\sqrt{2\pi\Delta t\,\mathrm{i}}}\exp\left(\mathrm{i}\frac{(\varphi^{n+1}-\varphi^n)^2}{2\Delta t}-\frac{\mathrm{i}\Delta t}{2}\omega^2(\varphi^n)^2+\mathrm{i}\Delta t J\varphi^n\right)\right\}. \end{aligned} \tag{2.9}$$

Here $\varphi^{N+1}$ can be regarded as the value of $\varphi$ as $t\to\infty$, which does not affect our analysis.

We perform a change of integration variables by replacing all $\varphi^n$ with $\sqrt{\mathrm{i}}\,u^n$, which leaves $K$ unchanged. This yields:

$$\begin{aligned} K &= \prod_{n=0}^{N}\left\{\int_{-\infty}^{\infty}\frac{\mathrm{d}u^n}{\sqrt{2\pi\Delta t}}\exp\left(-\frac{(u^{n+1}-u^n)^2}{2\Delta t}+\frac{1}{2}\omega^2(u^n)^2\,\Delta t+\mathrm{i}^{3/2}Ju^n\,\Delta t\right)\right\} \\ &= \prod_{n=0}^{N}\left\{\int_{-\infty}^{\infty}\frac{\mathrm{d}u^n}{\sqrt{2\pi\Delta t}}\exp\left[-\frac{(u^{n+1}-u^n)^2}{2\Delta t}\right]\cdot\exp\left(\frac{1}{2}\omega^2(u^n)^2\,\Delta t+\mathrm{i}^{3/2}Ju^n\,\Delta t\right)\right\} \end{aligned} \tag{2.10}$$

It can be seen that each factor inside the product corresponds to a Gaussian measure. In probabilistic terms, each field variable $u^n$ is a normally distributed random variable with mean equal to the next variable $u^{n+1}$ and standard deviation $\sqrt{\Delta t}$. The probabilistic interpretation of the above expression is to take a mathematical expectation over the potential and coupling terms. Since the integration over $u^n$ involves both $(u^{n+1}-u^n)^2$ and $(u^n-u^{n-1})^2$, the expectation is conditional. Hence, (2.10) can be written in the form of a conditional expectation:

$$K=\prod_{n=0}^{N}\left\{\mathbb{E}\left[\exp\left(\frac{1}{2}\omega^2(u^n)^2\,\Delta t+\mathrm{i}^{3/2}Ju^n\Delta t\right)\middle|u^{n-1},u^{n+1}\right]\right\}. \tag{2.11}$$

Alternatively, it can be expressed as a recursive chain:

$$K^{n+1} = \mathbb{E}\left[K^n \exp\left(\frac{1}{2}\omega^2 (u^n)^2\,\Delta t + \mathrm{i}^{3/2} J u^n \Delta t\right)\middle| u^{n+1}\right], \quad (n = 0, \cdots, N). \tag{2.12}$$

This constitutes the stochastic formulation of the path integral.

Since the variables $u^n$ are defined on distinct time intervals, they are mutually independent, and the sequence $\{u^n\}$ forms a Markov chain. In the limit $N \to \infty$ and $\Delta t \to 0$, $\{u^n\}$ converges to a continuous Wiener process (Brownian motion), defined by the following stochastic differential equation:

$$\mathrm{d}u = \sigma\,\mathrm{d}w(t), \tag{2.13}$$

where $w = w(t)$ is a Brownian motion and the volatility parameter $\sigma > 0$ is a constant introduced for later convenience (for (2.10), $\sigma = 1$). In fact, this expression suggests that the evolution and coupling of bosons can be described by more elaborate models. In general, $u$ can be represented as an Ornstein–Uhlenbeck process driven by multiple Brownian motions:

$$\mathrm{d}u = -\alpha(u - c)\mathrm{d}t + \sum_k \sigma_k\,\mathrm{d}w_k(t), \tag{2.14}$$

with $\alpha$ is a mean-reversion parameter, and $c$ represents a long term final state that $\varphi_T \to \sqrt{\mathrm{i}}\,c$ when $T \to \infty$. Thus, (2.14) introduces additional variables and parameters to describe more complex particle evolution. This effectively augments the field $\varphi$ with extra degrees of freedom: $\varphi = \varphi(t, w_1, w_2, \dots)$, compensating for the simplification of spatial dependence introduced by the localized excitation assumption.

Using the tower property of conditional expectations, the factors in (2.11) can be combined, and the final amplitude can be expressed as:

$$K = \mathbb{E}\left[\exp\left\{\int_{t_0}^{T}\left(\frac{1}{2}\omega^2 u(t,w)^2 + \mathrm{i}^{3/2} J u(t,w)\right)\mathrm{d}t\right\}\right], \tag{2.15}$$

where the expectation $\mathbb{E}$ is taken over all Wiener process (Brownian motion) sample paths $u(t, w)$ defined by (2.13) or (2.14). This equation indicates that for solving "point-to-point" transition amplitudes from an initial state $|\phi_0, t_0\rangle$ to a final state $|\phi_T, T\rangle$, it is not necessary to compute an expectation at each time step $t^n$. Instead, we integrate the function to be averaged along the sample paths prescribed by the Wiener process, evaluate the function at

each Gaussian-distributed point at the final time $T$, and then take a single expectation. In other words, we can integrate along Wiener paths to obtain the distribution $K^T(\varphi)$ of $K$ at time $T$, which corresponds to a "point-to-surface" transition amplitude. We define this evolution operation as $\mathbb{K}$:

$$K^T(\varphi) = \mathbb{K}^u\left[\exp\left\{\int_{t_0}^{T}\Big(\frac{1}{2}\omega^2 u(t,w)^2 + \mathrm{i}^{3/2}Ju(t,w)\Big)\mathrm{d}t\right\}\right]. \tag{2.16}$$

Referring to (2.12), we can iteratively compute $K^n(u)$ by a conditional evolution at each time $t^n$ as

$$K^{n+1}(\varphi) = \mathbb{K}^u\left[\exp\Big(\frac{1}{2}\omega^2 u(t,w)^2\Delta t + \mathrm{i}^{3/2}Ju(t,w)\Delta t\Big)\Big|\, t^n\right]K^n(\varphi), \quad (n=0,1,\cdots), \tag{2.17}$$

where the scalar $K^n(\varphi)$ is written on the right so that the same notation can be naturally extended to the matrix case. This stochastic formulation of the Feynman path integral provides a rigorous theoretical foundation for performing large-scale numerical simulations.

To the end of this section, we have three remarks:

First, the substitution $\varphi = \sqrt{\mathrm{i}}\,u$ should not be confused with the Wick rotation. Wick rotation transforms real time to imaginary time, $t \to -\mathrm{i}\tau$, mapping the Minkowski path integral to the Feynman-Kac formula [6], where the weight becomes real and positive-definite Euclidean weight $e^{-S_E}$. This turns the quantum problem into a classical statistical mechanics system, at the cost of losing real-time information. In contrast, our transformation acts on the field variable rather than time. The kinetic term is absorbed into the Wiener measure, while the potential term contributes a real factor $e^{\frac{1}{2}\omega^2 u^2\Delta t}$ in the exponential weight. The interaction terms introduce factors of $\mathrm{i}^{3/2} = e^{\mathrm{i}3\pi/4}$, which have both real and imaginary parts. Consequently, the total weight remains complex, preserving quantum coherence and real-time dynamics. Our formulation is therefore not equivalent to a Euclidean statistical description.

Second, as seen from (2.16), the transition amplitude $K$ is a function of time $T$ and the bosonic field configuration $\varphi$. Since $\varphi$ is driven by Brownian motion, the dependence of $K^T(\varphi)$ on $\varphi$ exhibits a Gaussian-like distribution profile, which greatly facilitates the numerical evolution of $K$. However, it is crucial to emphasize that this distribution arises from the auxiliary stochastic process and is fundamentally distinct from the probability density

defined in the quantum mechanical Hilbert space: $|K^T(\varphi)|^2$ is not the quantum mechanical probability density. The physical probability (or total transition amplitude) defined in quantum mechanics is independent of specific stochastic trajectories of $\varphi$. Its correct evaluation requires taking the expectation value of $K^T(\varphi)$ with respect to the Brownian motion measure (i.e., integrating over all $\varphi$), as given by:

$$\|K^T\| = \Big| \int_{-\infty}^{\infty} K^T(\varphi) \mathrm{d}\varphi \Big|. \tag{2.18}$$

Third, historically, Ord [7] and Jacobson & Schulman [8] also proposed a stochastic approach. In their work, stochastic terms are artificially added to the Euler–Lagrange equations of motion, leading to an Ornstein–Uhlenbeck process with drift terms given by the potential and the external source. It can be seen that their model equations not only deviate from Feynman's original conception of the path integral, but also alter the physical meaning of the parameters (such as $\omega$) in the system under study. Therefore, their approach is distinct from the one presented here.

# 3 Numerical scheme for the scalar field

Numerical methods for stochastic processes generally fall into two categories: Tree-grid methods and Monte Carlo methods, both of which are efficient approaches for solving scalar-field path integral problems. To explore more general bosonic evolution, we extend our study beyond the simple Wiener process (2.13) to the following Ornstein-Uhlenbeck process with a mean-reverting term:

$$\mathrm{d}u = -\alpha u \, \mathrm{d}t + \sigma \, \mathrm{d}w(t). \tag{3.1}$$

The physical interpretation of this evolution equation is that the bosonic field is excited from the vacuum state ($u = 0$) and gradually returns to the vacuum after a period of evolution. When the mean-reversion parameter $\alpha = 0$, we recover the original Wiener process.

## 3.1 Tree-grid method

The tree-grid method is analogous to the finite-difference schemes used in computational fluid dynamics. Briefly stated, the continuous field variable $u(t, w)$ is discretized into a

fixed set of grid points $\{u_i^n\}$ at different times $t^n$ and states $w_i$ over the evolution period. Using the evolution law given by (3.1), we construct the transition probabilities for $u$ moving between discrete points, as well as the survival probabilities upon reaching grid points. The transition amplitude and other results are then obtained by integrating along the paths in this probabilistic field according to (2.17).

The implementation of the grid method proceeds through the following steps:

Step 1. Discretize the evolution interval $[t_0, T]$ into small subintervals of length $\Delta t$. For simplicity, we assume uniform $\Delta t$; non-uniform partitions can be treated similarly. Denote the $n$-th time point as $t^n = t_0 + n\Delta t$.

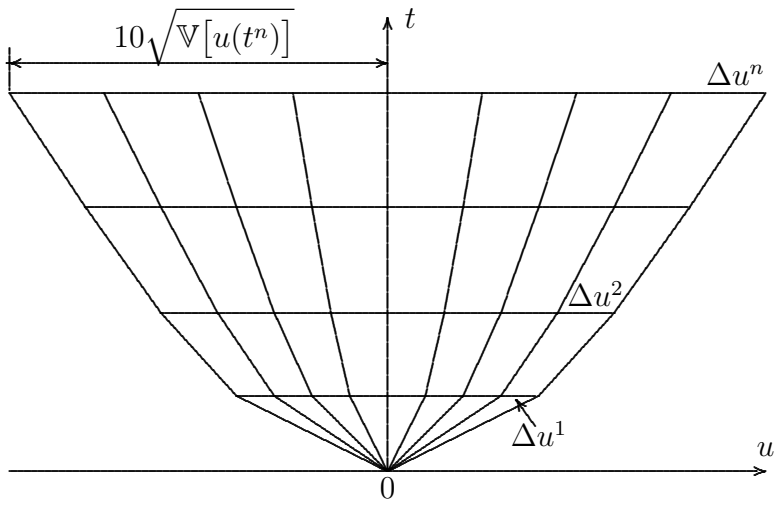


Figure 3.1: Diagram of a tree-structured grid.

Step 2. Construct the state grid for $u$. According to (3.1), the range of $u$ expands with increasing time $t$ under the influence of Brownian motion. The distribution of the $u$ grid is symmetric about the center $u = 0$. In the limiting case where $\alpha = 0$, the total width of the grid for $u$ at time $t$ is proportional to the standard deviation $\sqrt{\mathbb{V}[u(t)]} = \sigma\sqrt{t}$. Thus, at each time layer $t^n$, we center the grid at $u = 0$ and take a total width of $20\sqrt{\mathbb{V}[u]}$ (i.e., extending $10\sqrt{\mathbb{V}[u]}$ on each side). This interval is then divided uniformly into $2I$ segments, yielding $2I + 1$ equally spaced spatial grid points (we have chosen $I = 500$ in the following calculation example):

$$u_i^n = i\,\Delta u^n = i\left(\frac{10\sigma\sqrt{t^n}}{I}\right), \qquad (i = 0, \pm 1, \pm 2, \ldots, \pm I). \tag{3.2}$$

This results in a tree-like $u$-grid, as illustrated in Figure 3.1.

We emphasize that selecting the number of grid points $I$ and the grid spacing $\Delta u^n$ is critical for successful calculations. In our study, we dynamically monitor these parameters during computation for each specific problem, ensuring that the number of grid points is large enough to avoid boundary effects, and the grid spacing is fine enough to accurately resolve the simulated function distribution.

Step 3. Once the grid points are defined, we use the model equation to construct the transition probabilities for the amplitude. A multi-branch tree is employed to simulate the Brownian increment $\mathrm{d}w$. For an $m$-branch tree, the possible increments of $\mathrm{d}w$ over a time step $\Delta t$ and their corresponding transition probabilities can be written as

$$\Delta w_k = \frac{2k-m-1}{\sqrt{m-1}}\sqrt{\Delta t}, \qquad p_k = \frac{1}{2^{m-1}}\frac{(m-1)!}{(k-1)!\,(m-k)!}, \\ (k = 1, 2, \ldots, m). \tag{3.3}$$

Here, we illustrate the method using a four-branch tree as an example. According to the model equation (3.1) together with (3.3), the state $u_i^n$ can reach four intermediate points at time $t^{n+1}$ after a step $\Delta t$:

$$\begin{aligned} u_{\pm 1} &= (1-\alpha\Delta t)\,u_i^n \pm \frac{1}{\sqrt{3}}\,\sigma\sqrt{\Delta t}, \\ u_{\pm 2} &= (1-\alpha\Delta t)\,u_i^n \pm \sqrt{3}\,\sigma\sqrt{\Delta t}, \end{aligned} \tag{3.4}$$

where the transition probabilities of reaching $u_{+1}$ or $u_{-1}$ are $3/8$, and those of reaching $u_{+2}$ or $u_{-2}$ are $1/8$, as shown in Figure 3.2.

In general, the intermediate points do not coincide exactly with the grid points at time $t^{n+1}$. For each intermediate point, we locate its three nearest neighboring grid points and redistribute the transition probability to these three grid points, thereby obtaining the grid-to-grid transition probabilities. For example, consider the intermediate point $u_{+2}$. Let $u_k^{n+1}$ be the closest grid point and define

$$\eta = \frac{u_{+2} - u_k^{n+1}}{\Delta u^{n+1}}. \tag{3.5}$$

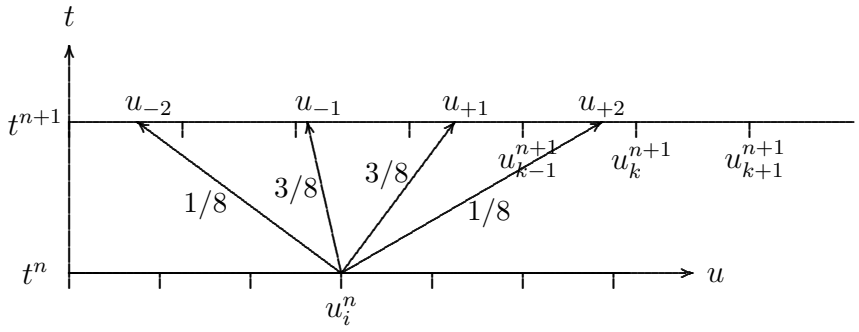


Figure 3.2: Transition probability between grid points.

Using a second-order Taylor expansion, the value of a function $f(t^{n+1}, u)$ at $u = u_{+2}$ can be expressed as

$$\begin{aligned} f_{+2} &= f_k^{n+1} + \frac{\eta}{2}\big(f_{k+1}^{n+1} - f_{k-1}^{n+1}\big) + \frac{\eta^2}{2}\big(f_{k+1}^{n+1} - 2f_k^{n+1} + f_{k-1}^{n+1}\big) \\ &= \frac{1}{2}\big(\eta^2 - \eta\big) f_{k-1}^{n+1} + \big(1 - \eta^2\big) f_k^{n+1} + \frac{1}{2}\big(\eta^2 + \eta\big) f_{k+1}^{n+1}. \end{aligned} \tag{3.6}$$

Guided by this Taylor expansion, we assign the following transition probabilities from the intermediate point $u_{+2}$ to the three neighboring grid points $u_{k-1}^{n+1}$, $u_k^{n+1}$, $u_{k+1}^{n+1}$:

$$\frac{1}{2}\big(\eta^2 - \eta\big), \qquad \big(1 - \eta^2\big), \qquad \frac{1}{2}\big(\eta^2 + \eta\big). \tag{3.7}$$

Multiplying each of these by 1/8 gives the transition probabilities from the starting grid point $u_i^n$ via $u_{+2}$ to the three target grid points. Repeating this procedure for the other three intermediate points $u_{+1}, u_{-1}, u_{-2}$ and summing the contributions yields the complete set of transition probabilities from $u_i^n$ to all grid points at time $t^{n+1}$.

We now provide a proof of the convergence and stability of the above algorithm. According to the requirements of stochastic analysis, this requires demonstrating that, within a time step $\Delta t$, the multi-branch tree scheme described above yields the same mathematical expectation and variance as the model equation (3.1). In the case of the four-branch tree described above, the mathematical expectation is

$$\mathbb{E}\Big[u_k^{n+1} \,\Big|\, u_i^n\Big] = \frac{3}{8}u_{+1} + \frac{3}{8}u_{-1} + \frac{1}{8}u_{+2} + \frac{1}{8}u_{-2} = u_i^n. \tag{3.8}$$

and the variance is

$$\mathbb{V}\Big[u_k^{n+1}\,\Big|\,u_i^n\Big] \;=\; \frac{3}{8}(u_{+1}-u_i^n)^2+\frac{3}{8}(u_{-1}-u_i^n)^2 + \frac{1}{8}(u_{+2}-u_i^n)^2+\frac{1}{8}(u_{-2}-u_i^n)^2 \;=\; \sigma^2\Delta t. \tag{3.9}$$

Therefore, the expectation and variance values given by the four-branch tree scheme are in complete agreement with the model equation. Clearly, the multi-branch tree implemented using (3.3) can also yield the same results. Thus, the above multi-branch tree scheme is convergent and stable.

Step 4. Compute the evolution of the system's transition amplitude. According to (2.17), the transition amplitude is obtained by integrating along the paths of $u$. Therefore, while calculating the grid-to-grid transition probabilities for $u$, we also compute the amplitude at each grid point along the transferred paths.

Let $K_i^n$ denote the amplitude at grid point $i$ at time level $n$, and let $p_{ik}^n$ be the transition probability from grid point $u_i^n$ to $u_k^{n+1}$. The contribution to the amplitude at grid point $k$ at time $t^{n+1}$ from this particular path is

$$(K_k^{n+1})_i = K_i^n\,\exp\Big(\frac{1}{2}\omega^2(u_i^n)^2\Delta t+\mathrm{i}^{3/2}J(t^n)u_i^n\Delta t\Big)\,p_{ik}^n. \tag{3.10}$$

Summing over all starting grid points $i$ at time level $n$ gives the total amplitude arriving at $u_k^{n+1}$:

$$K_k^{n+1}=\sum_{i=-I}^{I}K_i^n\,\exp\Big(\frac{1}{2}\omega^2(u_i^n)^2\Delta t+\mathrm{i}^{3/2}J(t^n)u_i^n\Delta t\Big)\,p_{ik}^n. \tag{3.11}$$

At this point, however, something appears to be missing. In the original path-integral expression (2.10), the computation at each time layer is sequential: the integrand for $u^n$ contains both $(u^{n+1}-u^n)^2$ and $(u^n-u^{n-1})^2$. Yet the construction of the update scheme in (3.11) uses only one of these terms. A correction is therefore necessary. For an $N$-fold Gaussian integral we have the exact result:

$$\prod_{n=1}^{N}\left\{\int_{-\infty}^{\infty}\frac{\mathrm{d}u^n}{\sqrt{2\pi\Delta t}}\exp\Big[-\frac{(u^{n+1}-u^n)^2}{2\Delta t}\Big]\right\}=\frac{1}{\sqrt{N}}. \tag{3.12}$$

Hence, when we iterate the scheme step by step, starting from the second layer ($n=2$), the update at the $n$-th layer should be multiplied by a factor $\sqrt{(n-1)/n}$ for correction.

Equation (3.11) is thus modified to

$$K_k^{n+1} = \sum_{i=-I}^{I} K_i^n \exp\Big(\frac{1}{2}\omega^2 (u_i^n)^2 \Delta t + \mathrm{i}^{3/2} J(t^n) u_i^n \Delta t\Big)\, p_{ik}^n \sqrt{\frac{n-1}{n}}. \tag{3.13}$$

Moreover, as remarked earlier, the integration at the $n = 0$ layer is fictitious, so the result for the $n = 1$ layer also requires adjustment. Note that at the initial time $t^0$ the amplitude is non-zero only at the origin $u_0^0 = 0$. Using the formula above, the amplitude at grid point $k$ in the first layer ($n = 1$) becomes

$$K_k^1 = \sum_{i=-I}^{I} K_i^0 \exp\Big(\frac{1}{2}\omega^2 (u_i^0)^2 \Delta t\Big) p_{ik}^0 = K_0^0\, p_{0k}^0. \tag{3.14}$$

On the other hand, the analytic expression for the transition amplitude from the point $u_0^0 = 0$ to $u_k^1$ after a short time $\Delta t$ can be derived from (3.22) as

$$K_k^1 = \frac{K_0^0}{\sqrt{\mathrm{i}}} \left[\frac{\Delta u^1}{\sqrt{2\pi \Delta t}} \exp\Big(-\frac{(u_k^1)^2}{2\Delta t}\Big)\right] \frac{1}{\Delta u^1}. \tag{3.15}$$

The term in square brackets can be interpreted as a transition probability. Comparing the two expressions, we see that the numerical computation of the amplitude $K_k^1$ at the first layer must be divided by the grid spacing $\Delta u^1$ of that layer, and the initial condition of $K_0^0$ needs to be divided by $\sqrt{\mathrm{i}}$ as well.

It can be seen that the transition amplitude $K_k^{n+1}$ in (3.13) contains three normalized factors: a constant $\sqrt{\mathrm{i}}$, the integral measure at time step $t^{n+1}$, i.e. $\mathrm{d}u^{n+1}$, and the survival probability of grid point $P_k^{n+1}$. In calculations with Yukawa or QED models, we usually need to separate these three factors. The first one, $\sqrt{\mathrm{i}}$, is a global constant that can be removed from the initial conditions. The second one can be obtained from the grid spacing: $\mathrm{d}u^{n+1} = u_{k+1}^{n+1} - u_k^{n+1}$. The last one must be calculated alongside the grid evolution. Let the survival probability at grid $k$ at time step $t^n$ be $P_k^n$. Once the transition probabilities $p_{kj}^n$ ($k, j = 1, 2, \dots$) from $t^n$ to $t^{n+1}$ are obtained from Step 3, the survival probability at $t^{n+1}$ can be computed as

$$P_j^{n+1} = \sum_k P_k^n\, p_{kj}^n. \tag{3.16}$$

Thus, by setting the initial survival probability at the origin to $P_0^0 = 1$, we can compute all survival probabilities.

Following the above procedure, we update the amplitudes iteratively for each time step $\Delta t$, thereby completing the evolution from $t_0$ to $T$. Finally, if one wishes to compute the probability weighted transition amplitude at a specific point $k$, the result is given by (3.13). If the total transition amplitude at time $T$ is desired, as defined in (2.18), we sum over all grid points:

$$\|K^T\| = \left| \sum_{k=-I}^{I} K_k^T \Delta u^T \right|. \tag{3.17}$$

Note the amplitude $K$ is a complex number, its modulus and phase should be computed accordingly.

## 3.2 Monte Carlo method

In contrast to the tree-grid method, the Monte Carlo method continuously generates new states $u_m^n$ along the evolution paths, where the transition probability from $u_m^n$ to $u_m^{n+1}$ is fixed to unity. The implementation procedure consists of the following steps.

Step 1: Time discretization. This step is the same as in the tree-grid method, yielding the time sequence $t^n = t_0 + n\Delta t$.

Step 2: Generation of state paths. Over a time step $\Delta t = t^{n+1} - t^n$, the Brownian motion can be represented as $\mathrm{d}w = \sqrt{\Delta t}\,\xi$, where $\xi \in \mathcal{N}(0,1)$ is a Gaussian random number. The evolution equation (3.1) is then discretized in time as

$$u^{n+1} = (1 - \alpha\Delta t)\, u^n + \sigma\sqrt{\Delta t}\,\xi^n. \tag{3.18}$$

We apply the above equation to generate $M$ paths for $u$. The initial condition is set to $u_m^0 = 0$ $(m = 1, 2, \ldots, M)$. Knowing the state values $u_m^n$ $(m = 1, 2, \ldots, M)$, we can update $u_m^{n+1}$ at the next time step $t^{n+1}$ by

$$u_m^{n+1} = (1 - \alpha\Delta t)\, u_m^n + \sigma\sqrt{\Delta t}\,\xi_m^n, \qquad (m = 1, 2, \ldots, M). \tag{3.19}$$

Step 3: Evolution of the transition amplitude. Let $K_m^n$ denote the amplitude along path $m$ at time level $n$. According to (2.17), the transition amplitude is obtained by integrating along the paths of $u$. Consequently, the update equation for the transition amplitude is

$$K_m^{n+1} = K_m^n \exp\left(\frac{1}{2}\omega^2 (u_m^n)^2 \Delta t + \mathrm{i}^{3/2} J(t^n) u_m^n \Delta t\right), \qquad (m = 1, 2, \ldots, M). \tag{3.20}$$

When the distribution of the transition amplitude $(u_m^n, K_m^n)$ $(m = 1, 2, \ldots, M)$ at time $t^n$ is known, the distribution $(u_m^{n+1}, K_m^{n+1})$ at time $t^{n+1}$ can be obtained by updating through (3.19) and (3.20). Then, we return to Step 2 for the next time step calculation.

### 3.3 Numerical examples

To validate the stochastic formulation for bosonic fields, we consider a classic example: a one-dimensional harmonic oscillator under a constant external source. The action is given by (2.5) with $J(t) = J_0$ being a constant source. We aim to compute the transition amplitude from $\varphi(0) = a$ to $\varphi(T) = b$:

$$K(b, T; a, 0) = \int \mathcal{D}\varphi \, e^{\mathrm{i}S[\varphi]}. \tag{3.21}$$

For a constant source, this path integral admits a closed-form solution. Following the method presented by Feynman and Hibbs [5], the analytic solution for the case $a = 0$ (i.e., starting from the vacuum state $\varphi = 0$) is

$$\begin{aligned} K(b, T; 0, 0) \;=\; & \sqrt{\frac{\omega}{2\pi \mathrm{i} \, \sin(\omega T)}} \cdot \exp\Bigg\{ \mathrm{i} \frac{b^2 \omega}{2} \frac{\cos(\omega T)}{\sin(\omega T)} \\ & + \mathrm{i} \frac{b J_0}{\omega} \frac{1 - \cos(\omega T)}{\sin(\omega T)} \;+\; \mathrm{i} \frac{J_0^2}{2\omega^3} \Big( \omega T - 2 \frac{1 - \cos(\omega T)}{\sin(\omega T)} \Big) \Bigg\}. \end{aligned} \tag{3.22}$$

The phase factor in this expression differs slightly from the result given by Feynman and Hibbs. Since this formula is crucial for validating our scheme, a detailed derivation is provided in the Appendix for the reader's reference.

First, we validate the tree-grid method with Wiener process against analytic solutions for the harmonic oscillator, where the mean-reversion parameter is set to $\alpha = 0$. Figures 3.3–3.6 demonstrate perfect agreement for both "closed-path" $(a = b = 0)$ and fixed-time $(b \neq 0)$ evolution scenarios. Regarding Figure 3.6, the observed discontinuities for large $J_0$ and $\omega$ are artifacts of the complex phase's multi-valued nature—purely mathematical features that can be readily handled in numerical implementation, rather than physical phenomena or method errors.

Notably, Figure 3.5 reveals an important feature of the external source $J$. In the absence of $J$, the even potential $u^2$ leads to a symmetric growth of the amplitude distribution. When $J = J_0$ is constant, or more generally when $J$ is an even function of $u$, the interaction term

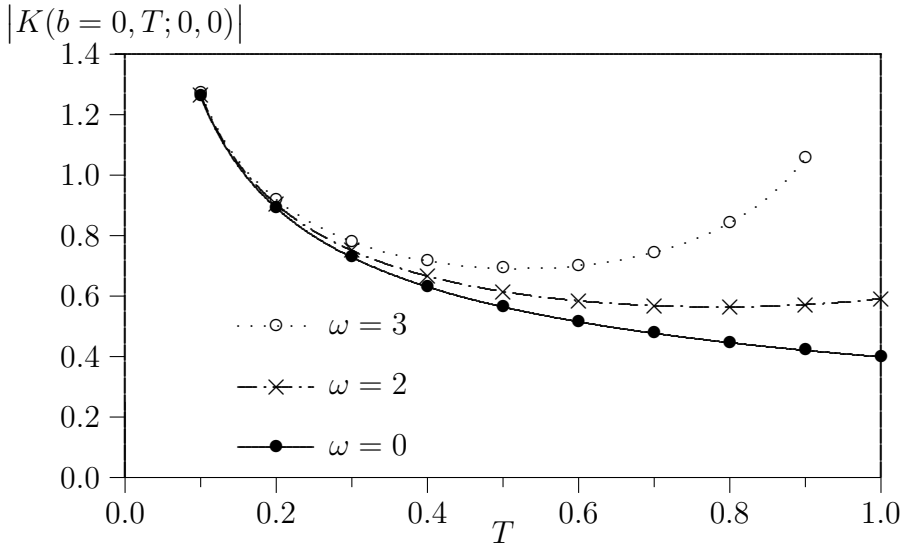


Figure 3.3: Magnitude of the transition amplitude $|K(b=0,T;0,0)|$ for the forced harmonic oscillator under a constant source. Lines: analytic; symbols: numerical.

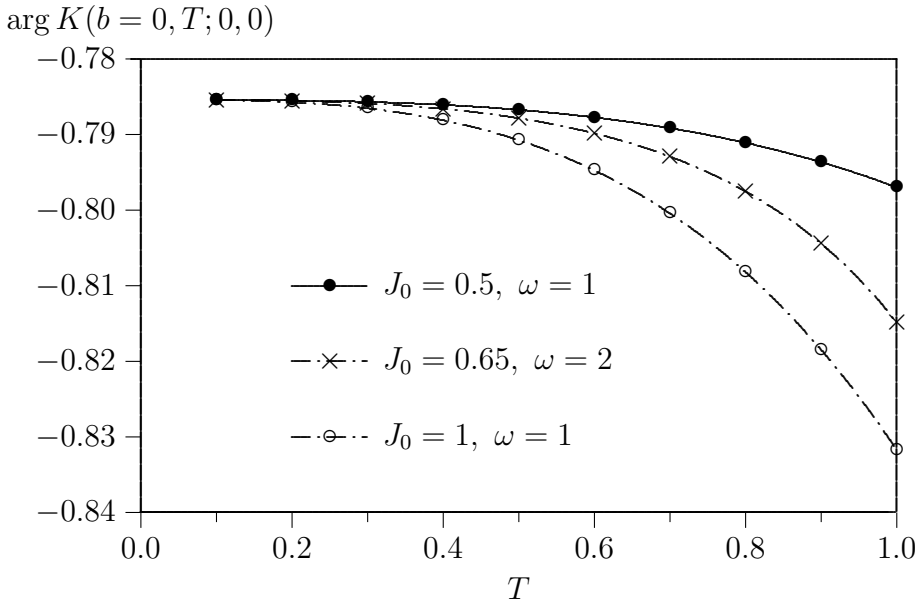


Figure 3.4: Phase of the transition amplitude $\arg K(b=0,T;0,0)$ for the forced harmonic oscillator under constant source. Lines: analytic; symbols: numerical.

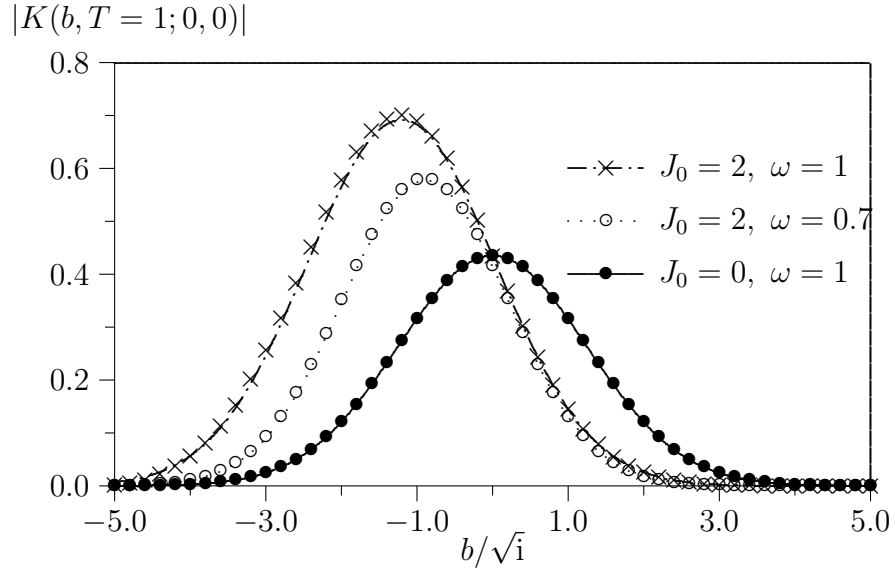


Figure 3.5: Magnitude of the transition amplitude $|K(b, T = 1; 0, 0)|$ for the forced harmonic oscillator under constant source. Lines: analytic; symbols: numerical.

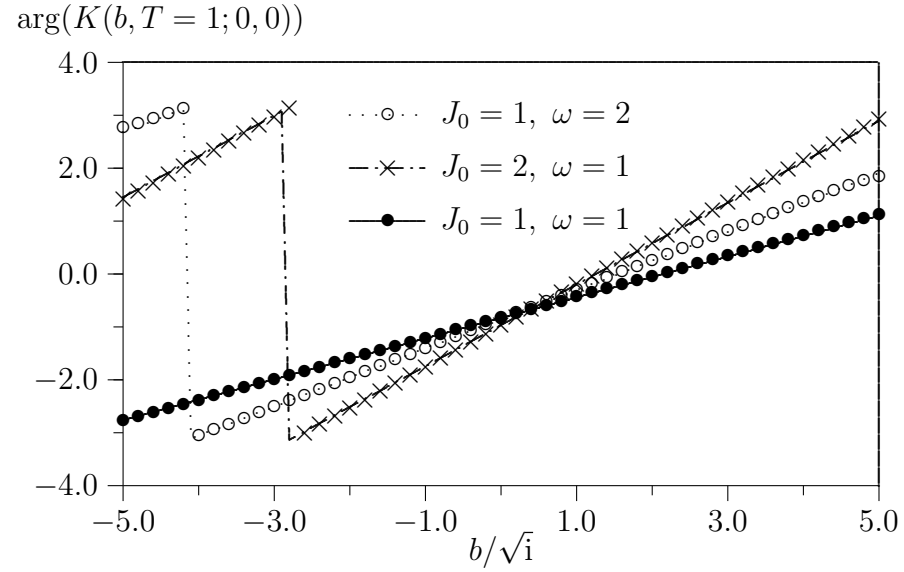


Figure 3.6: Phase of the transition amplitude $\arg(K(b, T = 1; 0, 0))$ for the forced harmonic oscillator under constant source. Lines: analytic; symbols: numerical.

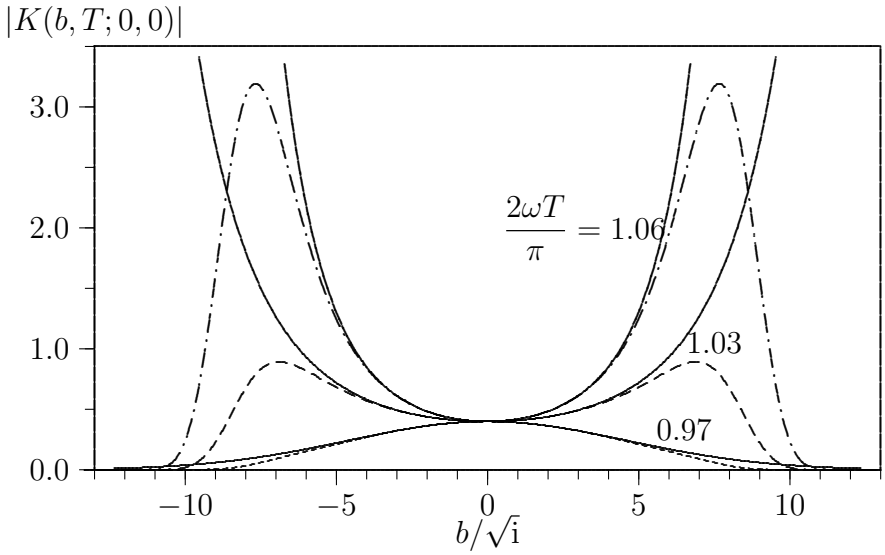


Figure 3.7: Magnitude of the transition amplitude $|K(b,T;0,0)|$ for the free scalar field harmonic oscillator near the critical time $\omega T = \pi/2$. Solid lines: analytic; dashed or dotted lines: numerical.

$Ju$ is odd, and the distribution shifts to one side: $J > 0$ shifts the distribution toward $\varphi < 0$, while $J < 0$ shifts it toward $\varphi > 0$. Conversely, when $J$ is an odd function of $u$ (so that $Ju$ is even), the distribution remains symmetric, either growing or contracting uniformly.

However, a critical feature arises in the free massive boson model: the "temporal singularity." As shown in Figure 3.7, at the critical time $T = \pi/(2\omega)$, the transition amplitude becomes independent of the final state. Consequently, the distribution transforms from bell-shaped to bowl-shaped (bimodal). This singularity effectively bounds the interaction time window for massive bosons.

To address this instability, we examine the standard Ornstein-Uhlenbeck process (3.1) with the mean-reversion parameter $\alpha = 1$. Unlike the free field, the mean-reversion term introduces a strong damping potential that suppresses large field excitations. As illustrated in Figure 3.8, this damping prevents the formation of bimodal distributions, ensuring a stable, bell-shaped distribution suitable for long-term evolution. In Figure 3.8, we also present the numerical results obtained from the Monte Carlo method, which agree very well with the tree-grid method at short times, although they lose accuracy as time increases.

Based on this section's presentation and numerical example, we compare the tree-grid and Monte Carlo methods. The Monte Carlo method is simpler and easier to implement,

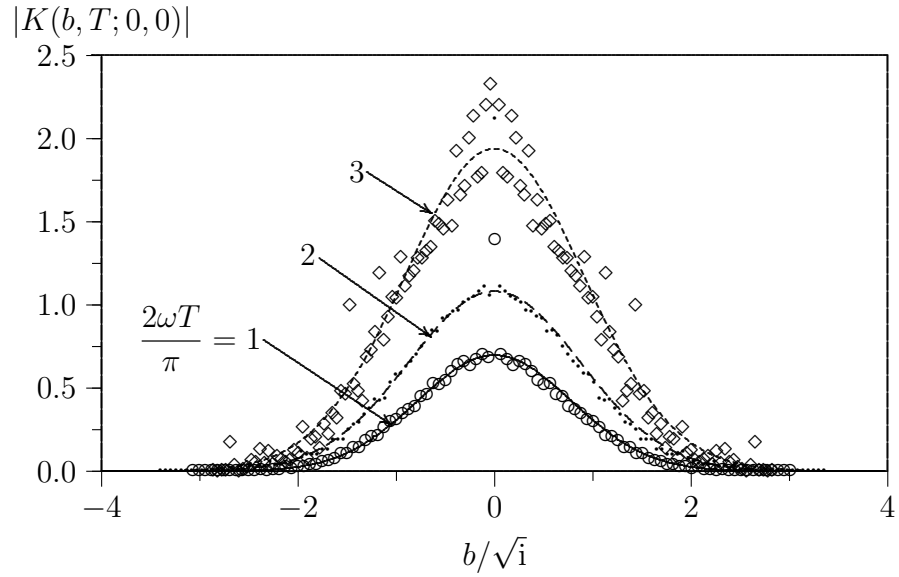


Figure 3.8: Magnitude of the transition amplitude $|K(b,T;0,0)|$ for the OU model with $\alpha = 1$ at different times $T$. Lines: grid method; symbols: Monte Carlo method.

making it suitable for large-scale simulations with many bosonic fields, such as those in QCD models. Although more complex, the tree-grid method offers higher accuracy and is indispensable for model validation and algorithm verification.

# 4 Stochastic formulation of the Dirac field

In quantum field theory, the Lagrangian for a free Dirac spinor field is given by

$$\mathcal{L} = \bar{\psi}\big(\mathrm{i}\gamma^{\mu}\partial_{\mu} - \lambda\big)\psi, \tag{4.1}$$

where, for later convenience in modeling with a Poisson process, we denote the spinor-field mass by $\lambda$.

The fermion field $\psi$ is a 4-component Dirac spinor. In the chiral (Weyl) representation, it can be decomposed into two irreducible 2-component Weyl spinors: a left-handed field $\psi_L(t,\vec{x})$ and a right-handed field $\psi_R(t,\vec{x})$, such that $\psi = (\psi_L, \psi_R)^T$. This decomposition is particularly suited for studying chiral symmetry and its breaking, which is a central theme of this work.

To focus on the internal dynamics induced by the mass term, we consider a spatially localized fermionic excitation and replace the spatial dependence with a stochastic variable.

This reduces the Weyl fields to time-dependent complex amplitudes $q_L(t), q_R(t) \in \mathbb{C}$. The fields can then be separated as

$$\psi_L(t,\vec{x}) = q_L(t)\,F(\vec{x}), \qquad \psi_R(t,\vec{x}) = q_R(t)\,F(\vec{x}), \tag{4.2}$$

where $F(\vec{x}) \in \mathbb{R}$ is a spherically symmetric, normalized real function satisfying

$$\int_{\mathbb{R}^3} F^2(\vec{x})\,\mathrm{d}^3x = 1, \qquad \int_{\mathbb{R}^3} F(\vec{x})\,\partial_i F(\vec{x})\,\mathrm{d}^3x = 0, \quad (i=1,2,3). \tag{4.3}$$

After performing the spatial integration, the classical action for the Lagrangian in (4.1) can be written as

$$\begin{aligned} S = \int \mathrm{d}t\mathrm{d}^3x\mathcal{L} &= \int \mathrm{d}t \left[\mathrm{i}q_L^\dagger(t)\dot{q}_L(t) + \mathrm{i}q_R^\dagger(t)\dot{q}_R(t) - \lambda\big(q_L^\dagger(t)q_R(t) + q_R^\dagger(t)q_L(t)\big)\right] \\ &= \int \mathrm{d}t \left[\mathrm{i}\vec{q}^{\,\dagger}(t)\dot{\vec{q}}(t) - \lambda\,\vec{q}^{\,\dagger}(t)\sigma_1\vec{q}(t)\right], \end{aligned} \tag{4.4}$$

where $\vec{q}(t)$ is a vector, and $\sigma_1$ is a matrix:

$$\vec{q}(t) = \begin{pmatrix} q_L(t) \\ q_R(t) \end{pmatrix}, \qquad \sigma_1 = \begin{pmatrix} 0 & 1 \\ 1 & 0 \end{pmatrix}. \tag{4.5}$$

The corresponding Euler–Lagrange equation of motion to (4.4) is

$$\mathrm{i}\frac{\mathrm{d}}{\mathrm{d}t}\begin{pmatrix} q_L \\ q_R \end{pmatrix} = \lambda\sigma_1 \begin{pmatrix} q_L \\ q_R \end{pmatrix} = \lambda \begin{pmatrix} q_R \\ q_L \end{pmatrix}. \tag{4.6}$$

From this moving equation we can see that the existence of $q_L$ implies a jump to $q_R$ with a factor of amplitude $-\mathrm{i}\lambda\mathrm{d}t$, and the existence of $q_R$ implies a jump to $q_L$ with the same factor. Thus, the underlying physical process is the coherent oscillations between the two components with frequency $\lambda$ (the quantum-mechanical Zitterbewegung). This exhibits the characteristic Dirac-type dynamics and can simulate the evolution of a fermionic state.

It is worth noting that the bilinear combination

$$j(t) := \vec{q}^{\,\dagger}(t)\sigma_1\vec{q}(t) = q_L^\dagger(t)q_R(t) + q_R^\dagger(t)q_L(t) = 2\,\mathrm{Re}(q_L^* q_R) \tag{4.7}$$

is precisely the projection of the scalar density $\psi_L^\dagger\psi_R + \mathrm{h.c.}$ of the original field theory under the localized excitation approximation (4.2):

$$\int \mathrm{d}^3x\ \psi_L^\dagger(t,\vec{x})\psi_R(t,\vec{x}) + \mathrm{h.c.} = j(t). \tag{4.8}$$

Consequently, this structure can also be naturally employed for Yukawa coupling with a scalar field $\varphi(t)$ (e.g., $-g\varphi j$), or as part of a vector current interacting with a gauge field.

We now search for a transition amplitude for the system, namely, a $2 \times 2$ matrix $K(\Delta t)$ which makes $\vec{q}(t)$ transits to

$$\vec{q}(t + \Delta t) = K(\Delta t)\vec{q}(t). \tag{4.9}$$

It is known from (4.6) that the transition of $\vec{q}(t)$ includes not only the continuous evolution of the two components $q_L$ and $q_R$, but also discrete jumps between these two components. Thus the transition amplitude $K(\Delta t)$ must be applicable both to continuous and jump.

To capture the jump stochastic nature, we model the dynamics as a continuous-time two-state Markov chain. Define a stochastic process $\xi(t) \in \{L, R\}$ that indicates the internal state of the system at time $t$. The process is driven by Poisson jumps with intensity $\lambda$, causing $\xi(t)$ to switch between the two states at random times. The total number of jumps up to time $t$, denoted by $N(t)$, follows a Poisson distribution:

$$\mathbb{P}(N(t) = n) = \frac{(\lambda t)^n}{n!} e^{-\lambda t}. \tag{4.10}$$

Motivated by the Euler–Lagrange equation (4.6): for a small time step $\Delta t$, the amplitude for a transition from $q_L$ to $q_R$ is $-\mathrm{i}\lambda\Delta t + \mathcal{O}(\Delta t^2)$, the leading-order transition amplitude is proportional to $-\mathrm{i}$. To capture this universal phase structure in the stochastic formulation, we assign a factor of $-\mathrm{i}$ to each jump event, while the jump rate $\lambda$ governs the probability of transitions. The amplitude from an initial state $\xi(0) = \alpha$ to a final state $\xi(t) = \beta$ is defined as the sum over all paths that start at $\alpha$ and end at $\beta$, each weighted by $(-\mathrm{i})^{N(t)}$. Motivated by the correspondence between the matrix $\sigma_1$ and the state switching, we postulate the following stochastic expectation for the transition amplitude:

$$K_{\beta\alpha}(t) = c\,\mathbb{E}_{\xi(0)=\alpha}\left[(-\mathrm{i})^{N(t)} \cdot \mathbf{1}_{\{\xi(t)=\beta\}}\right], \tag{4.11}$$

where $\mathbf{1}_{\{\xi(t)=\beta\}}$ is the indicator function equal to 1 if $\xi(t) = \beta$ and 0 otherwise. The constant $c$ is fixed by the requirement that the transition amplitude matrix $K(\Delta t)$ be unitary, $K^\dagger K = I$, which implies that each column must have unit norm:

$$\sum_{\beta=L,R} |K_{\beta\alpha}|^2 = 1, \qquad (\text{for } \alpha = L, R). \tag{4.12}$$

Let us consider the evolution from an initial state $\alpha$ to a final state $\beta$ over a short time interval $\Delta t = t - t_0$. Suppose the process $\xi(t)$ undergoes $n$ jumps during this interval. Because the system has only two states, $L$ and $R$, an odd number of jumps leads to a transition from $\alpha$ to $\beta$, while an even number of jumps returns the system to $\alpha$ (equivalent to no net transition). The transition amplitudes therefore take the form

$$\begin{aligned} K_{\alpha\alpha}(\Delta t) &= c\sum_{n=0}^{\infty}(-\mathrm{i})^{2n}\frac{(\lambda\Delta t)^{2n}}{(2n)!}e^{-\lambda\Delta t} = c\cos(\lambda\Delta t)e^{-\lambda\Delta t}, \\ K_{\beta\alpha}(\Delta t) &= c\sum_{n=0}^{\infty}(-\mathrm{i})^{2n+1}\frac{(\lambda\Delta t)^{2n+1}}{(2n+1)!}e^{-\lambda\Delta t} = -\mathrm{i}c\sin(\lambda\Delta t)e^{-\lambda\Delta t}. \end{aligned} \tag{4.13}$$

Using (4.12) for the transition process,

$$|K_{\alpha\alpha}(\Delta t)|^2 + |K_{\beta\alpha}(\Delta t)|^2 = (c\,e^{-\lambda\Delta t})^2 = 1, \tag{4.14}$$

which gives $|c| = e^{\lambda\Delta t}$. To fix the phase of $c$, we require the transition matrix to be unitary and to approach the identity matrix as $\Delta t \to 0$. This leads to the choice $c = e^{\lambda\Delta t}$ (the positive real solution). Consequently, the transition amplitudes become

$$K_{\alpha\alpha}(\Delta t) = \cos(\lambda\Delta t), \qquad K_{\beta\alpha}(\Delta t) = -\mathrm{i}\sin(\lambda\Delta t). \tag{4.15}$$

The complex phase factor $(-\mathrm{i})$ precisely represents the amplitude acquired when $\xi(t)$ jumps between different states.

We now turn to the transition amplitude for continuous evolution. Since the Euler–Lagrange equation (4.6) is a linear first-order differential equation with constant coefficient, its solution,

$$\vec{q}(t) = e^{-\mathrm{i}Ht}\vec{q}(0), \qquad H := \lambda\sigma_1, \tag{4.16}$$

defines a linear, unitary and continuous time evolution. This means that the dynamics of the system is fully determined by the initial state and the operator $K(t) = e^{-\mathrm{i}Ht}$. The evolution operator is

$$e^{-\mathrm{i}Ht} = e^{-\mathrm{i}\lambda t\sigma_1} = \sum_{k=0}^{\infty}\frac{1}{k!}(-\mathrm{i}\lambda t)^k\sigma_1^k = \cos(\lambda t)\,I - \mathrm{i}\sin(\lambda t)\,\sigma_1, \tag{4.17}$$

which exactly reproduces the amplitudes (4.15) obtained from the Poisson process. Thus, for both continuous and jump evolution, we have the transition amplitude matrix which,

similar to the bosonic scalar field case, also defines an evolution operator as

$$\vec{q}(t+\Delta t) = \mathbb{K}(\lambda\Delta t)\vec{q}(t) = \begin{pmatrix} \cos(\lambda\Delta t) & -\mathrm{i}\sin(\lambda\Delta t) \\ -\mathrm{i}\sin(\lambda\Delta t) & \cos(\lambda\Delta t) \end{pmatrix} \vec{q}(t). \tag{4.18}$$

Notably, this formulation achieves the unitary evolution of the spinor field using only complex numbers and Poisson statistics, completely bypassing the need for anti-commuting Grassmann variables.

# 5 Numerical scheme for the Dirac field

Based on the Poisson stochastic formulation of the spinor-field path integral, we now propose a corresponding numerical finite-difference scheme, enabling computer simulations of fermionic evolution in quantum field theory. This section examines a simple yet typical model: computing the physical transition probability $\mathbb{P}_{L\to R}$ for a two-state fermion under the influence of a classical scalar field $\phi_{\mathrm{cl}}(t)$ from the left-handed state $|L\rangle$ to the right-handed state $|R\rangle$, and comparing the result with perturbation theory in the weak-coupling regime ($g \ll 1$).

We assume that the scalar field is non-dynamical, modeled as a Gaussian pulse of a massless boson occurring at $t = 0$:

$$\phi_{\mathrm{cl}}(t) = e^{-t^2/(2\tau^2)}, \qquad \text{with } \tau = 1. \tag{5.1}$$

The Yukawa-type coupling term $-g\phi_{\mathrm{cl}}j$ corresponds in this model to the Lagrangian

$$\mathcal{L} \;=\; \mathrm{i}\vec{q}^{\,\dagger}(t)\dot{\vec{q}}(t) - g\phi_{\mathrm{cl}}(t)\,\vec{q}^{\,\dagger}(t)\sigma_1\vec{q}(t), \tag{5.2}$$

where we assume that the fermion is massless (i.e., no $\lambda\,\vec{q}^{\,\dagger}\sigma_1\vec{q}$ term) and the scalar field $\phi_{\mathrm{cl}}(t)$ is a prescribed classical external field. According to standard time-dependent perturbation theory [1], for this simple model, the first-order transition probability is given by

$$\mathbb{P}^{\mathrm{pert}}_{L\to R} = 2\pi g^2. \tag{5.3}$$

Following the stochastic formulation for the spinor field established in Section 4, we treat the evolution of this system as a continuous-time two-state Markov chain. Define an effective

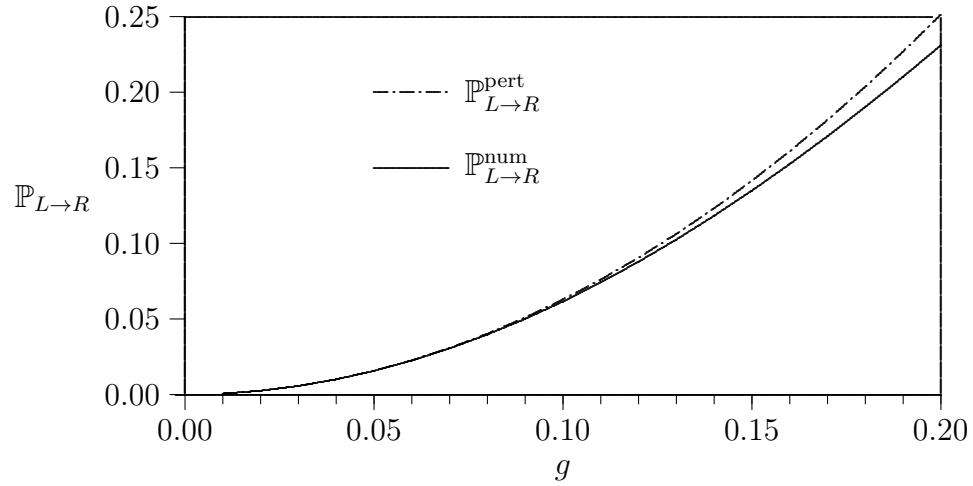


Figure 5.1: The transition probability of a fermion from left-hand state to right-hand state.

coupling strength

$$\lambda(t) = g\,\phi_{\rm cl}(t), \tag{5.4}$$

then we can use (4.18) to perform the evolution.

We choose a sufficiently large number $T$ to define the time interval $[-T, T]$ over which the evolution is simulated. We then discretize this interval into $2N$ equal time steps of length $\Delta t = T/N$, i.e.,

$$t^n = -T + n\Delta t, \qquad (n = 0, 1, \cdots, 2N). \tag{5.5}$$

Thus, we obtain the explicit finite-difference scheme:

$$\begin{aligned} q_L^{n+1} &= \cos(\lambda^n \Delta t)\, q_L^n - \mathrm{i}\sin(\lambda^n \Delta t)\, q_R^n, \\ q_R^{n+1} &= \cos(\lambda^n \Delta t)\, q_R^n - \mathrm{i}\sin(\lambda^n \Delta t)\, q_L^n, \end{aligned} \tag{5.6}$$

where $\lambda^n = g\,\phi_{\rm cl}(t^n)$, and the initial conditions are

$$q_L^0 = 1, \qquad q_R^0 = 0. \tag{5.7}$$

After $2N$ iterations we obtain the final state $q^{2N} = (q_L^{2N}, q_R^{2N})^T$. The physical transition probability from the left-handed state $|L\rangle$ to the right-handed state $|R\rangle$ is then given by the squared modulus of the amplitude on $|R\rangle$:

$$\mathbb{P}^{\rm num}_{L\to R} = \left|q_R^{2N}\right|^2. \tag{5.8}$$

Regarding numerical stability, the von Neumann analysis confirms that scheme (5.6) is unconditionally stable. However, to properly resolve the evolution of $\lambda(t)$ and avoid approximation errors, a sufficiently small time step is required. We perform simulations with $\Delta t = 0.001$ and integration limit $T = 10$, which effectively captures the dynamics over the entire real line. As shown in Figure 5.1, the numerical results align excellently with first-order perturbation theory (5.3) in the weak-coupling regime, validating the accuracy of the stochastic method.

# 6 Yukawa model and fermion mass

We now consider the case where a bosonic scalar field $\varphi$ and a fermionic spinor field $\vec{q} = (q_L, q_R)^T$ are coupled through the Yukawa model. Following the variable notation established in the preceding chapters, the Lagrangian of the system is expressed as

$$\mathcal{L} = \frac{1}{2}\dot{\varphi}^2 - \frac{1}{2}\omega^2\varphi^2 + \mathrm{i}\vec{q}^{\dagger}\dot{\vec{q}} - \lambda\,\vec{q}^{\dagger}\sigma_1\vec{q} - g\,\varphi\,\vec{q}^{\dagger}\sigma_1\vec{q}. \tag{6.1}$$

where $g$ is the Yukawa coupling constant. From a physical perspective, the Yukawa term plays a dual role: on one hand, it serves as the coupling between the fermionic internal transition $(\vec{q}^{\dagger}\sigma_1\vec{q})$ and the bosonic field, providing an effective external source $J = -g(\vec{q}^{\dagger}\sigma_1\vec{q})$ for the $\varphi$ field, thereby driving the distribution of the $\varphi$ field away from its symmetric center; on the other hand, this asymmetric distribution of the $\varphi$ field feeds back onto the fermion, correcting its effective mass from the initial mass $\lambda$ to $\lambda + g\varphi$, which in turn modulates the transition frequency between the two components of the fermion. This section demonstrates the applicability of our stochastic formulation to nonlinear and non-perturbative problems. We achieve this by calculating the dynamical evolution of the effective mass $\lambda_{\text{eff}}$ of the fermionic $\vec{q}$ field during the coupling process.

Let the joint transition amplitude of the system be $K = K^{\varphi,\vec{q}}$, whose evolution from $t_0$ to $T$ can be expressed using the Feynman path integral as

$$K^{\varphi,\vec{q}} = \int \mathcal{D}\varphi\,\mathcal{D}\vec{q}\,\exp\left\{\mathrm{i}\int_{t_0}^{T}\left(\frac{1}{2}\dot{\varphi}^2 - \frac{1}{2}\omega^2\varphi^2 + \mathrm{i}\vec{q}^{\dagger}\dot{\vec{q}} - \lambda\,\vec{q}^{\dagger}\sigma_1\vec{q} - g\,\varphi\,\vec{q}^{\dagger}\sigma_1\vec{q}\right)\right\}. \tag{6.2}$$

Within the framework of the stochastic formulation, this joint transition amplitude can be

decomposed into an iterative form of conditional evolutions:

$$K^{\varphi,\vec{q}}(t^{n+1}) \;=\; \mathbb{K}^{u,N}\left[\exp\Big(\frac{1}{2}\omega^2u^2\,\Delta t\Big)\cdot(-\mathrm{i})^{N(\lambda\Delta t)}\cdot\exp\Big(-\mathrm{i}g\varphi j\,\Delta t\Big)\,\Big|\,t^n\right]\,K^{\varphi,\vec{q}}(t^n),$$
$$(n=0,1,\cdots), \tag{6.3}$$

where $u=\mathrm{i}^{-1/2}\varphi$ is the Wiener or OU process, $N(\lambda\Delta t)$ is the total number of internal transitions of the $\vec{q}$ field within the time interval $\Delta t$, following a Poisson process with intensity $\lambda$, and $j=\vec{q}^{\dagger}\sigma_1\vec{q}$ is the transition current intensity of the fermionic field.

Since the $\vec{q}$ field is a two-dimensional spinor, the above equation is essentially a $2\times 2$ matrix equation. Introducing the wave function vector

$$\vec{f}(t;\varphi)=f_L(t;\varphi)|L\rangle+f_R(t;\varphi)|R\rangle=\begin{pmatrix}f_L(t;\varphi)\\ f_R(t;\varphi)\end{pmatrix}, \tag{6.4}$$

the equation can be rewritten in terms of two components:

$$\vec{f}(t^{n+1};\varphi) \;=\; \mathbb{K}^{u,N}\left[\exp\Big(\frac{1}{2}\omega^2u^2\,\Delta t\Big)\cdot(-\mathrm{i})^{N(\lambda\Delta t)}\cdot\exp\Big(-\mathrm{i}g\varphi j\,\Delta t\Big)\,\Big|\,t^n\right]\,\vec{f}(t^n;\varphi),$$
$$(n=0,1,\cdots). \tag{6.5}$$

To numerically implement the above evolution, we adopt the Strang splitting scheme [9], dividing each time step $[t^n,t^{n+1}]$ into two sub-steps:

$$\begin{aligned}\vec{f}(t^{n+1/2};\varphi) &= \mathbb{K}^{u}\left[\exp\Big(\frac{1}{2}\omega^2u^2\,\Delta t\;-\mathrm{i}^{3/2}guj\,\Delta t\Big)\right]\vec{f}(t^n;\varphi),\\ \vec{f}(t^{n+1};\varphi) &= \mathbb{K}^{N}\Big(\lambda\Delta t+g\varphi\Delta t\Big)\vec{f}(t^{n+1/2};\varphi).\end{aligned} \tag{6.6}$$

The first evolution operator $\mathbb{K}^u$ acts on the two components $f_L$ and $f_R$ of $\vec{f}$, modifying only their distribution along the $\varphi$ dimension without altering the relative relationship between the two components. It is worth noting that the source $j$ here differs from the fixed external source $J$ in Section 3, as it is dynamically determined by the wave function $\vec{q}(t^n;\varphi)$ at time step $t^n$:

$$j=\vec{q}^{\dagger}\sigma_1\vec{q}=q_L^*q_R+q_R^*q_L=2\,\mathrm{Re}(q_L^*q_R). \tag{6.7}$$

The vector $\vec{q}$ is derived from $\vec{f}$ using one of two methods, depending on how $\vec{f}$ is calculated. If the Monte Carlo method is used, $\vec{q}=\vec{f}$. If the tree-grid method is used, the three normalization factors in $\vec{f}$ must be removed.

In this calculation we focus on the coupling between a free fermion and a free boson. Both fields are initially symmetric. Thus, we choose the initial condition as

$$\vec{f}(0;0) = \begin{pmatrix} f_L(0;0) \\ f_R(0;0) \end{pmatrix} = \frac{1}{\sqrt{2}} \begin{pmatrix} 1+0\mathrm{i} \\ 1+0\mathrm{i} \end{pmatrix}, \tag{6.8}$$

while setting $\vec{f}(0;\varphi) = 0$ for $\varphi \neq 0$. Since $\mathbb{K}^u$ applies the same evolution to both components and $\mathbb{K}^N$ is a unitary operator, it is guaranteed that $f_L$ and $f_R$ remain equal throughout the evolution.

The second evolution operator $\mathbb{K}^N$ corresponds to the $2 \times 2$ matrix evolution established in Section 4, which performs internal mixing of $\vec{f}(t^{n+1/2};\varphi_k)$ at each fixed $\varphi_k$ without altering its distribution along the $\varphi$ dimension. The specific form is given by

$$\vec{f}(t^{n+1};\varphi) = \begin{pmatrix} \cos(\lambda_\varphi \Delta t) & -\mathrm{i}\sin(\lambda_\varphi \Delta t) \\ -\mathrm{i}\sin(\lambda_\varphi \Delta t) & \cos(\lambda_\varphi \Delta t) \end{pmatrix} \vec{f}(t^{n+1/2};\varphi), \tag{6.9}$$

where the effective frequency $\lambda_\varphi$ is given by comparing the mass term and interaction term in the Lagrangian (6.1):

$$\lambda_\varphi = \lambda + g\varphi. \tag{6.10}$$

From this, it can be seen that the bosonic field $\varphi$ modulates the effective mass of the fermion through its symmetry. At points where $\varphi > 0$, $\lambda_\varphi$ increases, while at points where $\varphi < 0$, $\lambda_\varphi$ decreases.

After evolving the wave function via $\mathbb{K}^N$ at a specific point $\varphi$, we calculate the fermionic current $j$ to drive the evolution of the $\varphi$ field in the subsequent time step. Assuming the Monte Carlo method is used to calculated $\vec{f}$, according to (6.7),

$$j(t^{n+1};\varphi) = \vec{f}^{\dagger}(t^{n+1};\varphi)\sigma_1 \vec{f}(t^{n+1};\varphi) =: J(\varphi). \tag{6.11}$$

Since $j$ depends on $\varphi$ that is symmetric, we decompose it into even and odd components for analysis:

$$j(t^{n+1};\varphi) := J_+(\varphi) + J_-(\varphi) = \frac{1}{2}\big(J(\varphi) + J(-\varphi)\big) + \frac{1}{2}\big(J(\varphi) - J(-\varphi)\big). \tag{6.12}$$

Based on the results in Figure 3.5, the even current $J_+$ modulates the shape of the $\varphi$ distribution: $J_+ < 0$ (implying a force $-gJ_+ > 0$) pushes the field toward the $\varphi \leq 0$ region,

whereas $J_+ > 0$ pushes it toward $\varphi \geq 0$. Conversely, the odd current $J_-$ couples to the bosonic mass term $\omega^2$, effectively scaling the width of the distribution: $J_- < 0$ leads to an expansion, while $J_- > 0$ results in a contraction. Thus, the influence of the fermionic current $j$ on the bosonic field is distinctly characterized by these two mechanisms.

Next, we discuss how to compute the fermion mass shift. Comparing the fermionic term and the interaction term in the Lagrangian (6.1), we find that on each evaluation path $m$, the instantaneous current is given by

$$-\lambda \left(\vec{q}_m^{\dagger} \sigma_1 \vec{q}_m\right) - g\varphi_m \left(\vec{q}_m^{\dagger} \sigma_1 \vec{q}_m\right), \tag{6.13}$$

where the first term is driven by the fermionic bare mass $\lambda$, and the second term is driven by the dynamical mass $g\varphi_m$ arising from the interaction.

Let the path probability be $p_m$ (for the tree-grid method, $p_m$ is the survival probability; for the Monte Carlo method, $p_m = 1/M$ is a constant). The expectation of the instantaneous current over all paths is then

$$-\lambda \sum_m p_m \left(\vec{q}_m^{\dagger} \sigma_1 \vec{q}_m\right) - g \sum_m p_m \varphi_m \left(\vec{q}_m^{\dagger} \sigma_1 \vec{q}_m\right). \tag{6.14}$$

Comparing the two terms in the above expression, we obtain the formula for the mass shift:

$$\delta\lambda = \frac{g \sum_m p_m \varphi_m \left(\vec{q}_m^{\dagger} \sigma_1 \vec{q}_m\right)}{\sum_m p_m \left(\vec{q}_m^{\dagger} \sigma_1 \vec{q}_m\right)}. \tag{6.15}$$

For comparison, classical perturbative quantum field theory provides the analytical expression for the mass shift under the one-loop approximation [10, 11]:

$$\delta\lambda_c(g, \omega, \lambda) = \frac{g^2 \lambda}{4\pi} \int_0^1 (1 - x) \, \ln\left[1 - x + \left(\frac{\omega}{\lambda}\right)^2 x^2\right] dx. \tag{6.16}$$

This expression indicates that in the weak-coupling regime, the mass shift is proportional to $g^2$ and $\lambda$, with its magnitude and sign determined by the ratio $\omega/\lambda$.

In Figures 6.1 we present the fermionic mass shift calculations using the stochastic method and compare them with perturbative results.

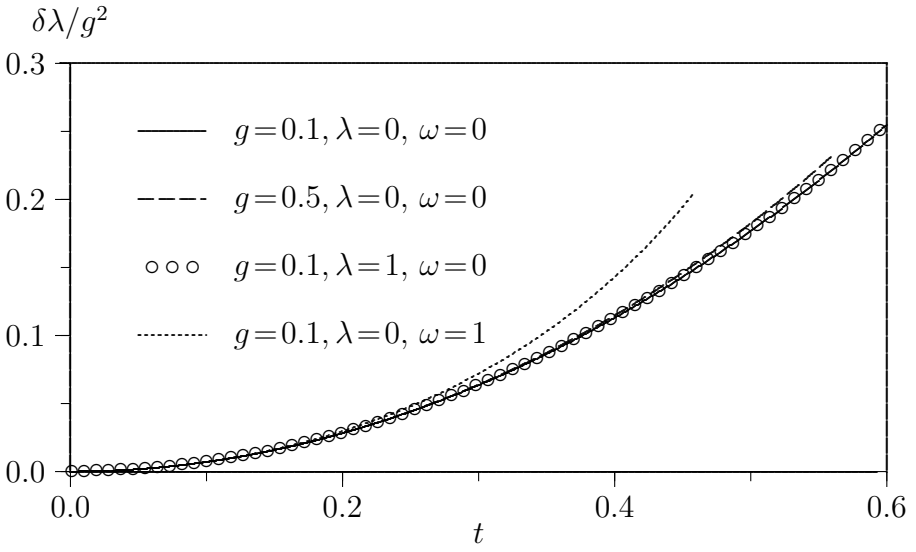


Figure 6.1: Normalized fermion mass shift $\delta\lambda/g^2$ as a function of time $t$ in the Yukawa model with a Wiener process.

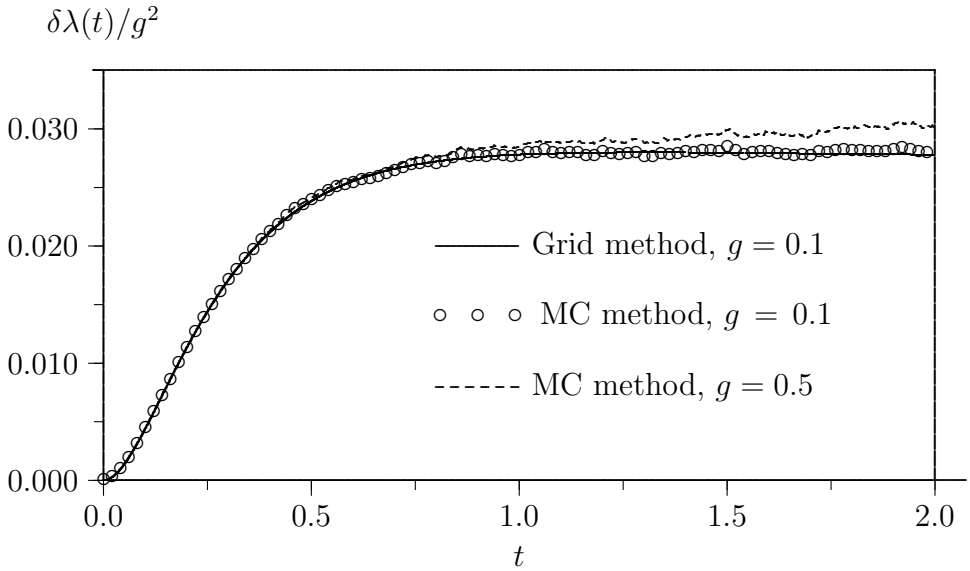


Figure 6.2: Normalized fermion mass shift $\delta\lambda/g^2$ as a function of time $t$ in the Yukawa model with an Ornstein-Uhlenbeck process (mean-reversion parameter $\alpha = 5$).

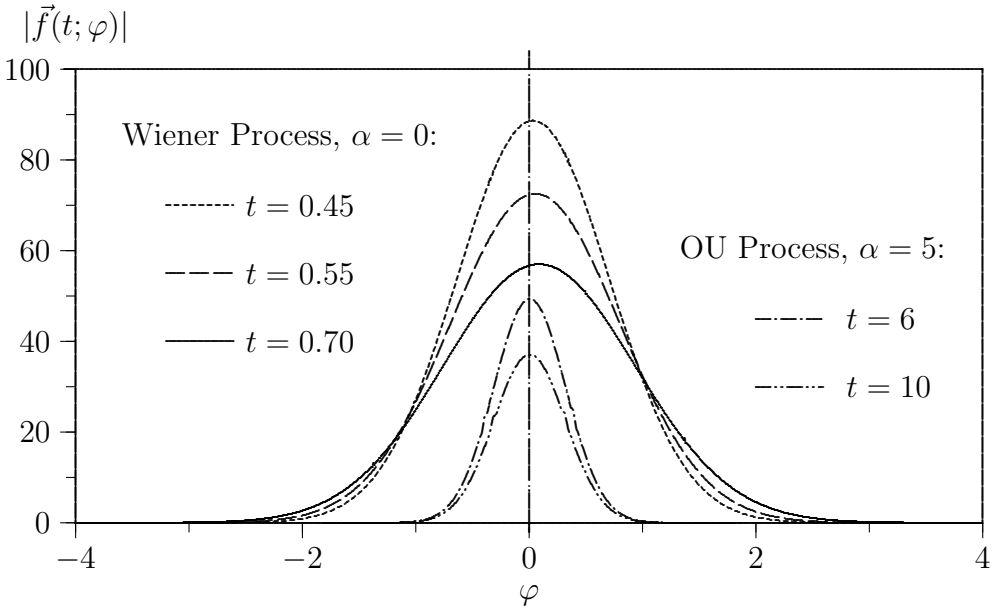


Figure 6.3: Wave function distribution $|\vec{f}(t;\varphi)|$ at different times $t$ in the Yukawa model. Parameters: $g = 0.5$, $\omega = 0$, $\lambda = 0$.

First, as shown in the figures, the mass shift $\delta\lambda$ initially exhibits a strict $g^2$ scaling, consistent with perturbation theory (6.16). However, as time progresses, small deviations arise due to higher-order contributions in $g$.

Second, Figure 6.1 reveals a significant feature of the stochastic method: $\delta\lambda$ is independent of the initial fermion mass $\lambda$. This independence contrasts sharply with perturbation theory and stems from the fact that the deformation of the $\varphi$ field is driven by the fermionic current $j$, which depends on the transition amplitude $\vec{q}$ rather than directly on $\lambda$. This independence also supports the fact that an initially massless fermion can acquire dynamical mass through evolution with bosons.

Finally, the figures also show that the bosonic mass $\omega$ has only a minor effect on $\delta\lambda$ and does not change the sign of $\delta\lambda$, which represents the direction of rotation in the two internal fermionic states.

Figure 6.1 shows that the mass acquired by the fermion increases without bound. As discussed earlier in Sections 2 and 3, the Wiener process represents a bosonic field that is excited from the vacuum state ($\varphi = 0$) and evolves arbitrarily without a definite destination. The bosonic transition amplitude expands and deforms indefinitely, which continuously

increases the fermionic mass.

To simulate the boson gradually returning to the vacuum state after a period of evolution, the Ornstein-Uhlenbeck process must be used. Figure 6.2 presents the fermion mass shift calculated in the Yukawa model using the Ornstein-Uhlenbeck process. This process introduces a restoring force that prevents the bosonic fields from diffusing indefinitely, thereby keeping the increase of the fermionic mass at a stable level.

Equation (6.15) shows that the fermionic mass shift depends on the asymmetry of the current $j = \vec{f}^{\dagger}\sigma_1\vec{f}$. Since the two components of $\vec{f}$ are same, we present the distribution of $|\vec{f}|$ along $\varphi$ at several time steps $t$ in Figure 6.3. For the Wiener process, the center of the wave profile indeed shifts toward the $\varphi > 0$ side. In the case of the OU process, due to the strong mean-reversion force, the wave profiles remain symmetric. This also explains how the fermionic mass is prevented from increasing indefinitely.

# 7 QED model and gauge interaction

Having validated the method on the scalar Yukawa interaction, we now extend the framework to the vector coupling present in QED. In quantum field theory, the Lagrangian of the QED model is given by

$$\mathcal{L} = \frac{1}{2}\big(\dot{\vec{A}}^2 - (\nabla \times \vec{A})^2\big) + \bar{\psi}\big(\mathrm{i}\gamma^0\partial_t + \mathrm{i}\vec{\gamma}\cdot\nabla - \lambda\big)\psi - \bar{\psi}\big(\hat{e}\gamma^\mu A_\mu\big)\psi. \tag{7.1}$$

To demonstrate the feasibility of the stochastic method in handling gauge interactions, we adopt a simplified scenario based on local excitation in field space, replacing the spatial coordinate dependence with a dependence on random variables. Assuming the spatial variation is concentrated near the origin, we decompose the fields into time-dependent amplitudes and a fixed spatial profile:

$$\vec{A}(t,\vec{x}) = \vec{\varphi}(t)F(\vec{x}) \;=\; \big(\varphi_1(t),\varphi_2(t),\varphi_3(t)\big)^T F(\vec{x}), \tag{7.2}$$

$$\psi(t,\vec{x}) = \vec{q}(t)F(\vec{x}) \;=\; \big(q_L(t),q_R(t)\big)^T F(\vec{x}), \tag{7.3}$$

where

$$F(\vec{x}) = \frac{(2\kappa)^{3/2}}{\sqrt{4\pi}}e^{-\kappa r}, \qquad r = |\vec{x}| \tag{7.4}$$

is a normalized, real, spherically symmetric function. Consequently, the kinetic and mass terms are reduced to effective quantum mechanical forms:

$$\frac{1}{2}\int_{\mathbb{R}^3} \mathrm{d}^3x \left(\dot{\vec{A}}^2 - (\nabla \times \vec{A})^2\right) = \frac{1}{2}\big(\dot{\varphi}_1^2 + \dot{\varphi}_2^2 + \dot{\varphi}_3^2\big) - \frac{2}{3}\kappa^2\big(\varphi_1^2 + \varphi_2^2 + \varphi_3^2\big), \tag{7.5}$$

$$\int_{\mathbb{R}^3} \mathrm{d}^3x\, \bar{\psi}\big(\mathrm{i}\gamma^0\partial_t + \mathrm{i}\vec{\gamma}\cdot\nabla - \lambda\big)\psi = \mathrm{i}\vec{q}^{\,\dagger}\dot{\vec{q}} - \vec{q}^{\,\dagger}(\lambda\sigma_1)\vec{q}, \tag{7.6}$$

$$\int_{\mathbb{R}^3} \mathrm{d}^3x\, \bar{\psi}\big(\hat{e}\gamma^\mu A_\mu\big)\psi = \sqrt{\frac{8\kappa^3}{\pi}}\hat{e}\ \vec{q}^{\,\dagger}\big(\varphi_0\sigma_0 + \varphi_1\sigma_1 + \varphi_2\sigma_2 + \varphi_3\sigma_3\big)\vec{q}. \tag{7.7}$$

In the above equations, $\sigma_\mu$ represent the standard Pauli matrices (with $\sigma_0$ as the identity):

$$\sigma_0 = \begin{pmatrix} 1 & 0 \\ 0 & 1 \end{pmatrix}, \quad \sigma_1 = \begin{pmatrix} 0 & 1 \\ 1 & 0 \end{pmatrix}, \quad \sigma_2 = \begin{pmatrix} 0 & -\mathrm{i} \\ \mathrm{i} & 0 \end{pmatrix}, \quad \sigma_3 = \begin{pmatrix} 1 & 0 \\ 0 & -1 \end{pmatrix}. \tag{7.8}$$

Let us set $\omega^2 = \kappa^2/3$ (with $\kappa = 0$ for massless photons) to match the single-boson Yukawa model, and introduce an effective charge $e = \sqrt{8\kappa^3/\pi}\,\hat{e}$. The resulting effective action reads:

$$\begin{aligned} S = \int \mathrm{d}^4x\, \mathcal{L} = \int_{t_0}^{t} \mathrm{d}t \Big[ & \frac{1}{2}\big(\dot{\varphi}_1^2 + \dot{\varphi}_2^2 + \dot{\varphi}_3^2\big) - \frac{\omega^2}{2}\big(\varphi_1^2 + \varphi_2^2 + \varphi_3^2\big) \\ & + \mathrm{i}\vec{q}^{\,\dagger}\dot{\vec{q}} - \vec{q}^{\,\dagger}(\lambda\sigma_1)\vec{q} - e\,\vec{q}^{\,\dagger}\big(\varphi_1\sigma_1 + \varphi_2\sigma_2 + \varphi_3\sigma_3\big)\vec{q}\Big]. \end{aligned} \tag{7.9}$$

Here, we adopt the radiation gauge ($\nabla \cdot \vec{A} = 0$) to eliminate the non-dynamical component $\varphi_0$ (which enforces Gauss's law), thereby focusing on the transverse degrees of freedom. This Abelian model serves as a proof of concept, and the same gauge-fixing strategy will be extended to non-Abelian gauge fields (SU(2) and SU(3)) in later sections.

Now we define a joint distribution wavefunction vector

$$\vec{f}(t;\vec{\varphi}) = \begin{pmatrix} f_L(t;\vec{\varphi}) \\ f_R(t;\vec{\varphi}) \end{pmatrix}, \tag{7.10}$$

to describe the evolution of the fermionic field $\vec{q}$. Within the framework of the stochastic formulation, the evolution of the three bosons $\varphi_1$, $\varphi_2$, and $\varphi_3$ can be simulated using three mutually independent Wiener processes (or Ornstein-Uhlenbeck processes). Following the application of the stochastic formulation in the Yukawa model, we can employ either the tree-grid method or the Monte Carlo method to solve for the evolution operators of the three bosons. If the tree-grid method is used, we apply the Strang splitting scheme [9] to

separate the three-dimensional operator into three one-dimensional operators:

$$\vec{f}(t+\Delta t/2;\vec{\varphi}+\Delta\varphi_k)=\mathbb{K}^{\varphi_k}\left[\exp\left(\frac{1}{2}\omega^2u_k^2\Delta t-\mathrm{i}^{3/2}e\,u_kj_k\Delta t\right)\Big|\,t^n\right]\vec{f}(t;\vec{\varphi}),$$
$$(k=1,2,3). \tag{7.11}$$

where the currents $j_1, j_2, j_3$ are obtained from the previous time step. Thus, the computer source code for one boson field evolution can be used repeatedly. If the Monte Carlo method is used, we first make the transformation $\vec{\varphi}=\sqrt{\mathrm{i}}\,\vec{u}$; then $\vec{u}$ follows a three-dimensional Wiener process (or OU process). On each Monte Carlo path $m$, the process can be simulated by Gaussian random numbers:

$$\vec{u}_m(t^{n+1})=(1-\alpha\Delta t)\vec{u}_m(t^n)+\sigma\sqrt{\Delta t}\,\vec{\xi}_m,\qquad \vec{\xi}_m\sim\mathcal{N}(0,I_3).$$

For simplicity, we omit the path label $m$ and rewrite the formula as:

$$\vec{u}(t^{n+1})=(1-\alpha\Delta t)\vec{u}(t^n)+\sigma\sqrt{\Delta t}\,\vec{\xi},\qquad \vec{\xi}\sim\mathcal{N}(0,I_3). \tag{7.12}$$

Thus, we obtain the coordinates $\vec{u}^{n+1}$ for $\vec{f}(t;\vec{\varphi})$ at the next time step $t=t^{n+1}$. The bosonic evolution of the two components of $\vec{f}$ takes the same form (also omitting the path label $m$):

$$\vec{f}(t^{n+1/2};\vec{\varphi}^{n+1})=\exp\left[\frac{\omega^2\Delta t}{2}\sum_{k=1}^{3}(u_k^n)^2-\mathrm{i}^{3/2}e\Delta t\sum_{k=1}^{3}(u_k^n)(j_k^n)\right]\vec{f}(t^n;\vec{\varphi}^n). \tag{7.13}$$

Based on Eq. (7.9), the Euler-Lagrange dynamical equation for $\vec{f}(t;\vec{\varphi})$ is given by

$$\mathrm{i}\dot{\vec{f}}=\left[(\lambda+e\varphi_1)\sigma_1+e\varphi_2\sigma_2+e\varphi_3\sigma_3\right]\vec{f}=(\vec{h}\cdot\vec{\sigma})\vec{f}, \tag{7.14}$$

where $\vec{h}=(\lambda+e\varphi_1,e\varphi_2,e\varphi_3)^T$ and $\vec{\sigma}=(\sigma_1,\sigma_2,\sigma_3)^T$. Within the framework of the stochastic formulation, the evolution equation for $\vec{f}$ reads

$$\vec{f}(t+\Delta t;\vec{\varphi})=\mathbb{K}^{\vec{q}}[\vec{f}(t;\vec{\varphi})]=e^{-\mathrm{i}(\vec{h}\cdot\vec{\sigma})\Delta t}\vec{f}(t;\vec{\varphi}). \tag{7.15}$$

Expanding $e^{-\mathrm{i}(\vec{h}\cdot\vec{\sigma})\Delta t}$ using Taylor's formula yields

$$e^{-\mathrm{i}(\vec{h}\cdot\vec{\sigma})\Delta t}=\cos(h\Delta t)\sigma_0-\mathrm{i}\frac{\sin(h\Delta t)}{h}(\vec{h}\cdot\vec{\sigma}), \tag{7.16}$$

where

$$h = |\vec{h}| = \sqrt{(\lambda + e\varphi_1)^2 + (e\varphi_2)^2 + (e\varphi_3)^2}. \tag{7.17}$$

Consequently, by substituting $\sigma_\mu$ into Eq. (7.16), we obtain the matrix form of the evolution equation for $\vec{f}$:

$$\vec{f}(t^{n+1}; \vec{\varphi}^{n+1}) = \begin{pmatrix} \cos\theta - \mathrm{i}\dfrac{h_3}{h}\sin\theta & -\mathrm{i}\dfrac{h_1 - \mathrm{i}h_2}{h}\sin\theta \\ -\mathrm{i}\dfrac{h_1 + \mathrm{i}h_2}{h}\sin\theta & \cos\theta + \mathrm{i}\dfrac{h_3}{h}\sin\theta \end{pmatrix} \vec{f}(t^{n+1/2}; \vec{\varphi}^{n+1}). \tag{7.18}$$

where $\theta = h\Delta t$. Once $\vec{f}$ is obtained, the three fermion-coupled currents are given by

$$j_1 = \vec{q}^{\,\dagger}\sigma_1\vec{q} = 2\,\mathrm{Re}(q_L^* q_R), \tag{7.19}$$

$$j_2 = \vec{q}^{\,\dagger}\sigma_2\vec{q} = 2\,\mathrm{Im}(q_L^* q_R), \tag{7.20}$$

$$j_3 = \vec{q}^{\,\dagger}\sigma_3\vec{q} = |q_L|^2 - |q_R|^2. \tag{7.21}$$

As in the Yukawa model, the vector $\vec{q}$ is derived from $\vec{f}$ in one of two ways depending on the method used. For the Monte Carlo method, $\vec{q} = \vec{f}$; for the tree-grid method, the three normalization factors in $\vec{f}$ must be removed. Once the currents are computed, the calculation cycle is complete and we proceed to the next time step.

Although the QED model involves three bosonic generators $\sigma_1$, $\sigma_2$, and $\sigma_3$, the governing equations show that the three directions play different roles. The $\sigma_1$ direction, which aligns with the fermionic mass, plays the dominant role. To justify this, consider the following example.

We calculate the dynamic flip probability of a fermionic electron between left-handed and right-handed states under the influence of massless bosonic photons. The parameters are chosen as follows: bosonic mass (treated as photon) $\omega = 0$, fermion mass $\lambda = 1$ and 0.5, and coupling constant $e = 0.01$. The initial conditions of $\vec{f}$ at $t = 0$ and at the origin $\vec{\varphi} = 0$ are set as

$$f_L(t = 0; \vec{\varphi} = 0) = 1, \qquad f_R(t = 0; \vec{\varphi} = 0) = 0. \tag{7.22}$$

At all other points where $\vec{\varphi} \neq 0$, we have

$$f_L(t = 0; \vec{\varphi}) = f_R(t = 0; \vec{\varphi}) = 0. \tag{7.23}$$

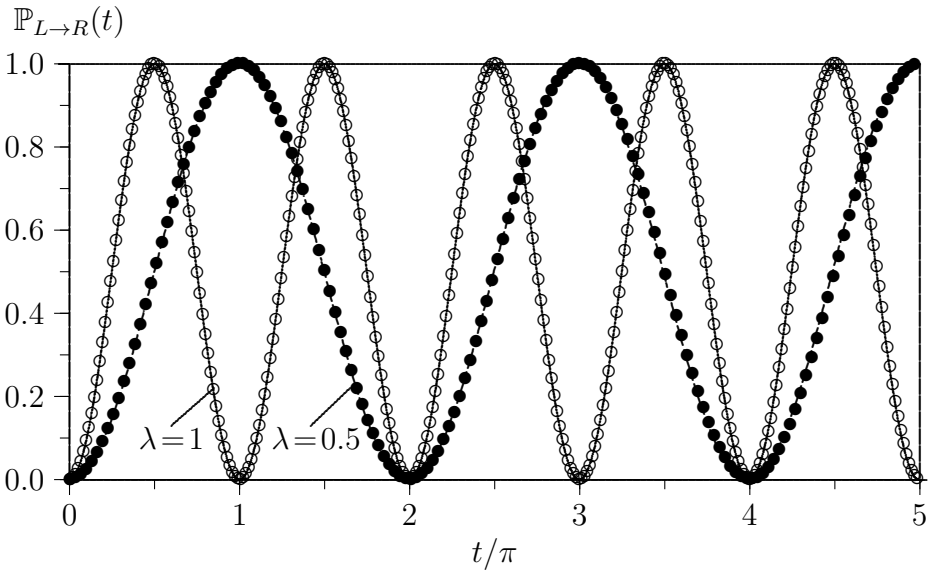


Figure 7.1: Dynamic transition probability of the fermion in the QED model from the left-handed state to the right-handed state. Parameters: $\omega = 0$, $\lambda = 1, 0.5$, and $e = 1$. Solid lines correspond to the Wiener process, while symbols correspond to the OU process with $\alpha = 5$.

According to (2.18), the physical flip probability we aim to compute is the squared modulus of the right-handed component of the wavefunction, given by

$$\mathbb{P}_{L\to R}(T) = \left| \iiint_{-\infty}^{\infty} f_R(T;\vec{\varphi})\,\mathrm{d}\varphi_1\,\mathrm{d}\varphi_2\,\mathrm{d}\varphi_3 \right|^2. \tag{7.24}$$

In the weak-coupling and short-time limit, using second-order perturbation theory can predict a linear growth for the average flip probability:

$$\mathbb{P}^{\mathrm{pert}}_{L\to R}(T) \approx C\,\hat{e}^2\,T, \tag{7.25}$$

where $C$ depends on the boson number. Unlike perturbation theory, the stochastic formulation imposes no restrictions on $e$ or $T$. While massive bosons ($\omega > 0$) exhibit a temporal singularity at $T = 2\pi/\omega$, massless photons ($\omega = 0$) do not, allowing for a complete description of the time evolution.

For comparison, we recall the theoretical prediction of the single-boson Yukawa model. In that model, symmetry constraints and the chosen initial conditions imply that the imaginary part of $f_L$ and the real part of $f_R$ remain zero throughout the evolution. Consequently, the

fermion-induced current $j_1$ vanishes, and the bosonic field remains undisturbed. The right-handed component then integrates to

$$q_R(\Delta t) = \int_{-\varphi_{\max}}^{\varphi_{\max}} f_R(\Delta t; \varphi)\, \mathrm{d}\varphi = \int_{-\varphi_{\max}}^{\varphi_{\max}} -\mathrm{i}\sin\left[(\lambda + g\varphi)\Delta t\right] \mathrm{d}\varphi \;\propto\; -\mathrm{i}\sin(\lambda \Delta t). \tag{7.26}$$

Thus, the Yukawa transition probability follows $\mathbb{P}_{L\to R}^{\text{Yukawa}} \propto \sin^2(\lambda t)$.

Remarkably, the QED model yields the same result as the Yukawa model. Figure 7.1 shows the computation from the stochastic formulation, where the flip probability curves take the form $\sin^2(\lambda t)$ with exactly $\lambda$ as the curve frequency. This justifies the previous statement. Meanwhile, the results also show that the behavior is independent of whether a Wiener process or an OU process is used to model the bosonic evolution.

As another numerical example, we compute the fermion mass shift in the QED model with the same initial conditions as in the Yukawa model. At $t = 0$, the bosonic fields begin to excite from the vacuum ($\vec{\varphi} = 0$), and

$$\vec{f}(0;0) = \begin{pmatrix} f_L(0;0) \\ f_R(0;0) \end{pmatrix} = \frac{1}{\sqrt{2}} \begin{pmatrix} 1 \\ 1 \end{pmatrix}. \tag{7.27}$$

Following a similar approach as in the Yukawa model, the fermion mass shift in the QED model is given by

$$\delta\lambda = \frac{e \sum_m p_m \big(\varphi_1 j_1 + \varphi_2 j_2 + \varphi_3 j_3\big)_m}{\sum_m p_m (j_1)_m}, \tag{7.28}$$

where $p_m$ is the survival probability of path $m$. For the tree-grid method, $p_m$ is obtained from the numerical evolution; for the Monte Carlo method, $p_m$ is constant and can be set to 1 for all paths.

The results are plotted in Figures 7.2 and 7.3 for the Wiener and OU approaches, respectively. Both results are identical to those of the Yukawa model. This is because $f_L$ and $f_R$ have the same initial condition and undergo identical evolution driven by the bosonic vector $\vec{\varphi}$; hence, $f_L = f_R$ holds throughout the evolution, and $j_2$ and $j_3$ remain zero. This consistency convincingly demonstrates the correctness of our implementation, successfully extending the stochastic formulation from simple one-dimensional models to complex higher-dimensional gauge theories.

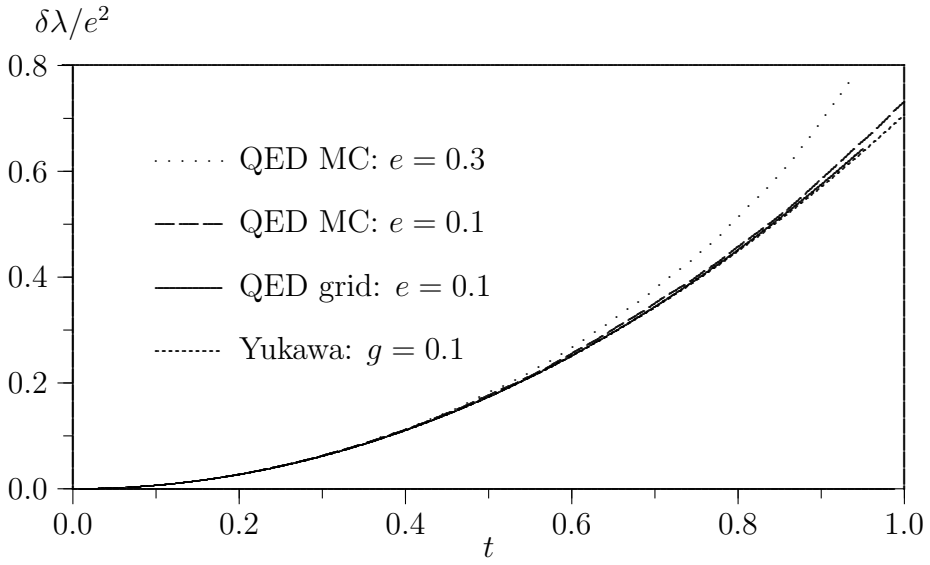


Figure 7.2: Normalized fermion mass shift $\delta\lambda/e^2$ as a function of time $t$ in the QED model with a Wiener process. Parameters: $\lambda = 0$, $\omega = 0$.

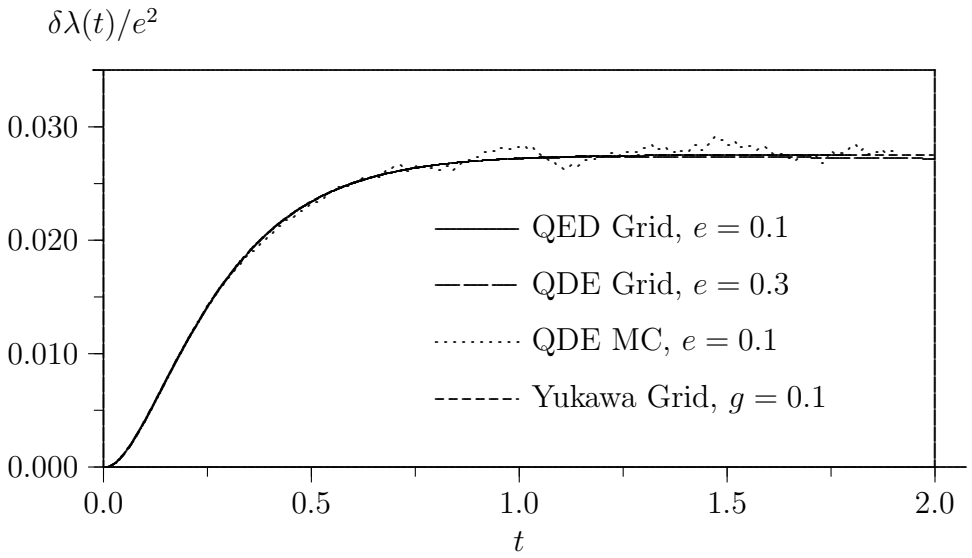


Figure 7.3: Normalized fermion mass shift $\delta\lambda/e^2$ as a function of time $t$ in the QED model with an Ornstein-Uhlenbeck process. Parameters: $\lambda = 0$, $\omega = 0$, $\alpha = 5$.

# 8 SU(2) Yang-Mills gauge field

We consider the coupling of Yang-Mills vector fields interacting with a fermion, for which the Lagrangian is expressed as [1]

$$\mathcal{L} = -\frac{1}{4}\big(F^a_{\mu\nu}\big)^2 + \bar{\psi}\big(\mathrm{i}\gamma^\mu D_\mu - \lambda\big)\psi, \tag{8.1}$$

where the field strength tensor $F^a_{\mu\nu}$ and the covariant derivative $D_\mu$ are defined as

$$F^a_{\mu\nu} = \partial_\mu A^a_\nu - \partial_\nu A^a_\mu + \hat{g}\epsilon^{abc} A^b_\mu A^c_\nu, \tag{8.2}$$

$$D_\mu = \partial_\mu - \mathrm{i}\hat{g}\frac{\sigma_a}{2} A^a_\mu. \tag{8.3}$$

Here, $\hat{g}$ is the coupling constant, $\sigma_a$ $(a = 1, 2, 3)$ are the Pauli matrices acting on the color space, $\gamma^\mu$ $(\mu = 0, 1, 2, 3)$ are the Dirac matrices, and $\epsilon^{abc}$ is the SU(2) structure constant.

We adopt the radiation (Coulomb) gauge condition by setting $A^a_0 = 0$ for $a = 1, 2, 3$. The remaining nine bosonic fields $A^a_i$ are grouped into three vectors according to the color index $a$:

$$\vec{A}^a = (A^a_1,\ A^a_2,\ A^a_3)^T, \qquad (a = 1, 2, 3). \tag{8.4}$$

Then, the Lagrangian in (8.1) can be written explicitly as

$$\begin{aligned}\mathcal{L} = {} & \frac{1}{2}\sum_{a=1}^{3}\big|\dot{\vec{A}}^a\big|^2 - \frac{1}{2}\sum_{a=1}^{3}\big|\nabla\times\vec{A}^a\big|^2 - \frac{\hat{g}^2}{4}\sum_{a,b=1}^{3}\Big(|\vec{A}^a|^2|\vec{A}^b|^2 - (\vec{A}^a\cdot\vec{A}^b)^2\Big) \\ & - \hat{g}\sum_{a,b,c=1}^{3}\sum_{i<j}\epsilon^{abc}(\partial_i A^a_j - \partial_j A^a_i)A^b_i A^c_j \\ & + \bar{\psi}\Big(\mathrm{i}\gamma^0\partial_0 + \mathrm{i}\vec{\gamma}\cdot\nabla - \lambda\Big)\psi + \bar{\psi}\Big(\frac{\hat{g}}{2}\sum_{a,i=1}^{3}\gamma^i\sigma_a A^a_i\Big)\psi.\end{aligned} \tag{8.5}$$

Here we have used the SU(2) identity $\epsilon^{abc}\epsilon^{ade} = \delta^{bd}\delta^{ce} - \delta^{be}\delta^{cd}$ to simplify the quartic term. The sum over $a, b$ runs over the three color directions. The combination $|\vec{A}^a|^2|\vec{A}^b|^2 - (\vec{A}^a\cdot\vec{A}^b)^2$ vanishes when $a = b$, i.e., when the gauge fields $\vec{A}^a$ and $\vec{A}^b$ are parallel in color space.

To set up a stochastic framework for the SU(2) Yang-Mills gauge field, we focus on a scenario where the field undergoes a localized excitation in space within a very short time interval. Consequently, the effective spatial variation of the fields can be assumed to be concentrated near the origin.

We decompose the gauge field $\vec{A}^a$ into a product of a spatial shape function and a time-dependent amplitude:

$$\vec{A}^a(t,\vec{x}) = F(\vec{x})\,\vec{\varphi}^a(t), \qquad (a=1,2,3), \tag{8.6}$$

where $\vec{\varphi}^a = (\varphi_1^a, \varphi_2^a, \varphi_3^a)^T \in \mathbb{R}^3$ is a function of time $t$, and $F(\vec{x})$ is a normalized, spherically symmetric spatial distribution function centered at the origin:

$$F(\vec{x}) = \sqrt{\frac{\kappa^3}{\pi}}\, e^{-\kappa r}, \qquad r = |\vec{x}|. \tag{8.7}$$

Taking the spatial integral of the gauge-field part of the Lagrangian density (8.5), the $A^3$ term vanishes because the terms involving $\partial_i A_j^a$ are odd in the spatial coordinates. Then we have

$$T_{\text{gauge}}(t) = \int_{\mathbb{R}^3} \mathrm{d}^3x\, \frac{1}{2}\sum_{a=1}^{3} \big|\dot{\vec{A}}^a\big|^2 = \frac{1}{2}\sum_{a=1}^{3} |\dot{\vec{\varphi}}^a|^2, \tag{8.8}$$

$$\begin{aligned} V_{\text{gauge}}(t) &= \int_{\mathbb{R}^3} \mathrm{d}^3x\, \frac{1}{2}\sum_{a=1}^{3} \big|\nabla\times\vec{A}^a\big|^2 + \int_{\mathbb{R}^3} \mathrm{d}^3x\, \frac{\hat{g}^2}{4}\sum_{a,b=1}^{3}\Big(|\vec{A}^a|^2\,|\vec{A}^b|^2 - (\vec{A}^a\cdot\vec{A}^b)^2\Big) \\ &= \frac{\kappa^2}{3}\sum_{a=1}^{3}|\vec{\varphi}^a|^2 + \frac{g^2}{16}\sum_{a<b}\Big(|\vec{\varphi}^a|^2\,|\vec{\varphi}^b|^2 - (\vec{\varphi}^a\cdot\vec{\varphi}^b)^2\Big), \end{aligned} \tag{8.9}$$

where we have introduced a new coupling constant $g = \sqrt{\kappa^3/\pi}\,\hat{g}$ in order to have a simple interaction term below. The summation over $a<b$ runs over the three color directions.

To focus on the coupling of the fermion field $\psi$ with the bosonic gauge fields, we consider $\psi$ in terms of its two spinorial degrees of freedom: a left-handed Weyl field $\psi_L(t,\vec{x})$ and a right-handed Weyl field $\psi_R(t,\vec{x})$, i.e., $\psi = (\psi_L, \psi_R)^T$. We also assume a localized spatial excitation, reducing the Weyl fields to a product of a spatial shape function and time-dependent complex amplitudes $\vec{q} = (q_L(t), q_R(t))^T \in \mathbb{C}^2$:

$$\psi(t,\vec{x}) = F(\vec{x})\,\vec{q}(t). \tag{8.10}$$

Performing the spatial integration for the fermionic part of the Lagrangian density (8.5), and noting that the term involving $\nabla\psi$ is odd in the spatial coordinates and thus integrates to zero, we obtain

$$L_{\text{fermi}}(t) = \int_{\mathbb{R}^3} \mathrm{d}^3x\, \bar{\psi}\big(\mathrm{i}\gamma^0\partial_0 + \mathrm{i}\vec{\gamma}\cdot\nabla - \lambda\big)\psi = \mathrm{i}\vec{q}^{\,\dagger}\dot{\vec{q}} - \vec{q}^{\,\dagger}\big(\lambda\sigma_1\big)\vec{q}. \tag{8.11}$$

For the interaction term, we work in the chiral representation, where

$$\gamma^0 = \begin{pmatrix} 0 & I \\ I & 0 \end{pmatrix}, \qquad \gamma^i = \begin{pmatrix} 0 & \sigma_i \\ \sigma_i & 0 \end{pmatrix}.$$

Thus, $\gamma^0\gamma^i = \mathrm{diag}(\sigma_i, \sigma_i)$ has diagonal blocks. Using the decomposition $\psi = (\psi_L, \psi_R)^T$ and $\bar{\psi} = \psi^\dagger\gamma^0$, we have

$$\bar{\psi}\gamma^i\sigma_a\psi = \psi_L^\dagger\sigma_i\sigma_a\psi_L + \psi_R^\dagger\sigma_i\sigma_a\psi_R.$$

Substituting the localized field ansatz $\psi_{L,R} = F(\vec{x})q_{L,R}$ and $\vec{A}^a = F(\vec{x})\vec{\varphi}^a$, and performing the spatial integration, we obtain

$$\begin{aligned} L_{\mathrm{int}}(t) &= \int_{\mathbb{R}^3} \mathrm{d}^3x\, \bar{\psi}\left(\frac{\hat{g}}{2}\sum_{a,i=1}^{3}\gamma^i\sigma_a A_i^a\right)\psi \\ &= \left(\int_{\mathbb{R}^3} F^3(\vec{x})\,\mathrm{d}^3x\right)\frac{\hat{g}}{2}\sum_{a,i=1}^{3}\left(q_L^\dagger\sigma_i\sigma_a q_L + q_R^\dagger\sigma_i\sigma_a q_R\right)\varphi_i^a \\ &= \frac{8g}{27}\,\vec{q}^\dagger\Big[(\varphi_1^1+\varphi_2^2+\varphi_3^3)I + \mathrm{i}(\varphi_2^3-\varphi_3^2)\sigma_1 + \mathrm{i}(\varphi_3^1-\varphi_1^3)\sigma_2 + \mathrm{i}(\varphi_1^2-\varphi_2^1)\sigma_3\Big]\vec{q}, \end{aligned} \tag{8.12}$$

where we have used the Pauli matrix identity $\sigma_i\sigma_a = \delta_{ia}I + \mathrm{i}\epsilon_{iak}\sigma_k$ and $\vec{q} = (q_L, q_R)^T$. Here $g$ is related to $\hat{g}$ as in (8.9).

Combining the expressions for the gauge kinetic term (8.8), the gauge potential term (8.9), the fermionic term (8.11), and the interaction term (8.12), we obtain the effective action for the SU(2) Yang-Mills model within the stochastic framework:

$$S(T) = \int \mathrm{d}^4x\,\mathcal{L} = \int_0^T \mathrm{d}t\left(T_{\mathrm{gauge}}(t) - V_{\mathrm{gauge}}(t) + L_{\mathrm{fermi}}(t) + L_{\mathrm{int}}(t)\right). \tag{8.13}$$

This action describes a finite-dimensional system of coupled bosonic variables $\vec{\varphi}^a(t) \in \mathbb{R}^3$ (one for each color generator) and fermionic variables $\vec{q}(t) \in \mathbb{C}^2$. The bosonic part retains the characteristic nonlinear self-interaction of SU(2) Yang-Mills theory, while the fermionic part exhibits a gauge-induced mass mixing. This formulation is well suited for stochastic quantization and can be solved numerically using Monte Carlo methods.

Now we derive the numerical scheme for the coupled evolution of the SU(2) Yang-Mills gauge field and the Dirac fermion. We define a wavefunction vector that depends on the bosonic configuration:

$$\vec{f}(t;\vec{\varphi}) = \begin{pmatrix} f_L(t;\vec{\varphi}) \\ f_R(t;\vec{\varphi}) \end{pmatrix}. \tag{8.14}$$

Here, the two components of $\vec{f}$ are functions of the SU(2) gauge field configuration $\vec{\varphi} = (\vec{\varphi}^1, \vec{\varphi}^2, \vec{\varphi}^3)^T$, evolving according to either Wiener or Ornstein-Uhlenbeck processes. Meanwhile, $f_L$ and $f_R$ correspond to the left- and right-handed components of the fermion, respectively, whose dynamics are described by a Poisson jump process.

To numerically implement the evolution of $\vec{f}$, we discretize time $t \geq 0$ into intervals of equal length $\Delta t$, denoted by $[t^n, t^{n+1}]$. At each time step $t^n$, the continuous bosonic field $\vec{\varphi}$ is discretized into $M$ independent states (or paths) $\vec{\varphi}_m$ $(m = 1, 2, \ldots, M)$. Thus, at each time $t^n$ we have $M$ independent samples of the wavefunction vector:

$$\vec{f}(t^n, \vec{\varphi}_m), \qquad (m = 1, 2, \ldots, M). \tag{8.15}$$

In the time direction, we employ a first-order operator splitting scheme to update $\vec{f}$ over $[t^n, t^{n+1}]$ in two steps. The first step updates $\vec{f}$ according to the bosonic evolution rule:

$$\vec{f}(t^{n+1/2}; \vec{\varphi}_m^{n+1}) = \mathbb{K}^{\vec{\varphi}}\Big[\vec{f}(t^n; \vec{\varphi}_m^n)\Big], \tag{8.16}$$

and the second step updates $\vec{f}$ according to the fermionic evolution rule:

$$\vec{f}(t^{n+1}; \vec{\varphi}_m^{n+1}) = \mathbb{K}^{\vec{q}}\Big[\vec{f}(t^{n+1/2}; \vec{\varphi}_m^{n+1})\Big]. \tag{8.17}$$

We first derive the explicit form of the first evolution operator $\mathbb{K}^{\vec{\varphi}}$.

In the stochastic formulation, the two components $f_L$ and $f_R$ of the fermion are driven by the three bosonic vectors $\vec{\varphi}^a$ (nine components in total). The evolution of these three bosonic vectors can be simulated by nine mutually independent Brownian motions. In numerical simulations, each Brownian motion corresponds to a one-dimensional array. Using the tree-grid method for high-dimensional Brownian motion would pose severe difficulties in programming and memory; therefore, we adopt the Monte Carlo method for computation.

In the simulation, we first apply the transformation $\vec{\varphi}^a = \sqrt{\mathrm{i}}\,\vec{u}^a$ to the Lagrangian; then $\vec{u}^a$ follows a three-dimensional Ornstein-Uhlenbeck process. On each Monte Carlo path $m$, time is discretized with step size $\Delta t$, and the OU process is simulated using Gaussian random numbers:

$$\vec{u}_m^a(t^{n+1}) = (1 - \alpha\Delta t)\,\vec{u}_m^a(t^n) + \sigma\sqrt{\Delta t}\,\vec{\xi}_m^a, \qquad \vec{\xi}_m^a \sim \mathcal{N}(0, I_3), \tag{8.18}$$

where the volatility parameter is set to $\sigma = 1$, and the mean-reversion parameter $\alpha$ is to be determined. This gives the "coordinates" for $\vec{f}(t^{n+1}; \vec{\varphi}_m^{n+1})$ at the next time step.

According to the stochastic representation, the bosonic evolution equation is given by

$$\vec{f}(t^{n+1/2}; \vec{\varphi}_m^{n+1}) = \mathbb{K}^{\vec{\varphi}}\Big[\vec{f}(t^n; \vec{\varphi}_m^n)\Big] = \exp\Big( - \mathrm{i}\Delta t V_{\text{gauge}} + \mathrm{i}\Delta t L_{\text{int}}\Big)\ \vec{f}(t^n; \vec{\varphi}_m^n). \tag{8.19}$$

Substituting $\vec{u}_m^a(t^n)$ into the above expression and omitting the path index $m$ for brevity, we obtain the updated wavefunction vector:

$$\vec{f}(t^{n+1/2}; \vec{\varphi}^{n+1}) = \exp\Big(A + B + C\Big)\ \vec{f}(t^n; \vec{\varphi}^n), \tag{8.20}$$

where

$$A = \frac{\kappa^2}{3}\Delta t \sum_{a=1}^{3} |\vec{u}^a|^2,$$

$$B = \mathrm{i}\frac{g^2}{16}\Delta t \sum_{a<b} \Big(|\vec{u}^a|^2|\vec{u}^b|^2 - (\vec{u}^a \cdot \vec{u}^b)^2\Big),$$

$$C = \mathrm{i}^{3/2}\frac{8g}{27}\Delta t\Big((u_1^1 + u_2^2 + u_3^3)j_0 + \mathrm{i}(u_2^3 - u_3^2)j_1 + \mathrm{i}(u_3^1 - u_1^3)j_2 + \mathrm{i}(u_1^2 - u_2^1)j_3\Big).$$

Here, the fermionic currents $j_0, j_1, j_2, j_3$ are obtained from the wavefunction $\vec{f}(t^n; \vec{\varphi}^n)$ at the previous time step, as will be specified in (8.28) below.

We now derive the second evolution operator $\mathbb{K}^{\vec{q}}$. Based on (8.11) and (8.12), the Euler-Lagrange equation for the fermionic wave vector $\vec{f}(t; \vec{\varphi})$ is given by

$$\mathrm{i}\dot{\vec{f}} = \Big[h_0 I + \lambda\sigma_1 + \mathrm{i}\big(\vec{h} \cdot \vec{\sigma}\big)\Big]\vec{f}, \tag{8.21}$$

where

$$h_0 = \frac{8g}{27}(\varphi_1^1 + \varphi_2^2 + \varphi_3^3), \qquad \vec{h} = \frac{8g}{27}\begin{pmatrix}\varphi_2^3 - \varphi_3^2\\ \varphi_3^1 - \varphi_1^3\\ \varphi_1^2 - \varphi_2^1\end{pmatrix}, \qquad \vec{\sigma} = \begin{pmatrix}\sigma_1\\ \sigma_2\\ \sigma_3\end{pmatrix}, \tag{8.22}$$

and $\frac{8g}{27}$ is the effective coupling constant after spatial integration.

Following the numerical scheme of the stochastic formulation used in the Yukawa and QED models, (8.21) yields the evolution equation for $\vec{f}$:

$$\vec{f}(t + \Delta t; \vec{\varphi}) = \exp\Big( - \mathrm{i}h_0\Delta t I - \mathrm{i}\lambda\Delta t\sigma_1 + (\vec{h} \cdot \vec{\sigma})\Delta t\Big)\ \vec{f}(t; \vec{\varphi}). \tag{8.23}$$

In the above expression, since the evolution along the bosonic dimension has already been completed, we have omitted the superscripts and subscripts of $\vec{\varphi}_m^{n+1}$ for simplicity.

The explicit presence of $\sigma_1$ in the above equation prevents us from further simplifying the evolution equation following the Yukawa approach. Therefore, in this paper we focus on the problem of dynamical fermion mass generation and set the bare mass $\lambda = 0$ (the chiral limit). The evolution equation then simplifies to

$$\vec{f}(t + \Delta t; \vec{\varphi}) = \exp\Big( - \mathrm{i} h_0 \Delta t I + (\vec{h} \cdot \vec{\sigma}) \Delta t \Big) \, \vec{f}(t; \vec{\varphi}). \tag{8.24}$$

Since $I$ commutes with $\vec{\sigma}$, the exponential can be factorized as

$$\vec{f}(t + \Delta t; \vec{\varphi}) = e^{-\mathrm{i} h_0 \Delta t} \, \exp\big( (\vec{h} \cdot \vec{\sigma}) \Delta t \big) \, \vec{f}(t; \vec{\varphi}). \tag{8.25}$$

Using the Pauli matrix identity $(\vec{h} \cdot \vec{\sigma})^2 = |\vec{h}|^2 I$, the second factor expands to

$$\exp\big( (\vec{h} \cdot \vec{\sigma}) \Delta t \big) = \cosh(\theta) I + \frac{\sinh(\theta)}{|\vec{h}|} (\vec{h} \cdot \vec{\sigma}), \tag{8.26}$$

where $\theta = |\vec{h}| \Delta t$. Consequently, the matrix form of the evolution equation for $\vec{f}$ is

$$\vec{f}(t^{n+1}; \vec{\varphi}) = e^{-\mathrm{i} h_0 \Delta t} \begin{pmatrix} \cosh\theta + \dfrac{h_3}{|\vec{h}|} \sinh\theta & \dfrac{h_1 - \mathrm{i} h_2}{|\vec{h}|} \sinh\theta \\ \dfrac{h_1 + \mathrm{i} h_2}{|\vec{h}|} \sinh\theta & \cosh\theta - \dfrac{h_3}{|\vec{h}|} \sinh\theta \end{pmatrix} \vec{f}(t^{n+1/2}; \vec{\varphi}), \tag{8.27}$$

where $h_1, h_2, h_3$ are the three components of $\vec{h}$, and $|\vec{h}| = \sqrt{h_1^2 + h_2^2 + h_3^2}$. Note that hyperbolic functions cosh and sinh appear here instead of trigonometric functions, because the exponent contains real coefficients. This reflects the fact that in the chiral limit ($\lambda = 0$), the evolution is dominated by real exponentials, which may lead to exponential growth of the path weights.

The fermionic evolution in this SU(2) model is very similar in form to that in the Yukawa and QED models. However, as can be seen from (8.27), the evolution is driven by nine bosonic components. Three of them appear in the phase factor $h_0$. This, as will be seen shortly, makes it easier to generate a dynamical fermion mass and to induce dynamical chiral symmetry breaking, compared to the Yukawa model and QED model in which only one bosen drives the fermion mass generation. The remaining six bosonic components form $\vec{h}$. They

appear in the arguments of the hyperbolic functions and can significantly drive the evolution of the wave vector. This reflects the richer dynamics inherent in non-Abelian gauge fields.

When the fermionic evolution is finished, we can compute the fermionic currents using the two-component nature of the wavefunction. Since the Monte Carlo method is used to simulate the bosonic evolution, we can directly use $\vec{f}$ to compute the currents without converting them to $\vec{q}$. The formulas are:

$$\begin{aligned} j_0 &= \vec{f}^\dagger \sigma_0 \vec{f} = |f_L|^2 + |f_R|^2, \\ j_1 &= \vec{f}^\dagger \sigma_1 \vec{f} = 2\,\mathrm{Re}(f_L^* f_R), \\ j_2 &= \vec{f}^\dagger \sigma_2 \vec{f} = 2\,\mathrm{Im}(f_L^* f_R), \\ j_3 &= \vec{f}^\dagger \sigma_3 \vec{f} = |f_L|^2 - |f_R|^2. \end{aligned} \tag{8.28}$$

Clearly, for each configuration $\vec{\varphi}_m^{n+1}$ $(m = 1, \ldots, M)$, we can construct a set of $h_0, h_1, h_2, h_3$; and for each pair $(f_L(t^{n+1}, \vec{\varphi}_m^{n+1}), f_R(t^{n+1}, \vec{\varphi}_m^{n+1}))$, we obtain a set of fermionic currents $j_0, j_1, j_2, j_3$. They provide the necessary input for computing $\vec{f}$ in the next time step via (8.20).

As an application of the stochastic Yang-Mills model developed in this chapter, we simulate the mass generation of a Dirac fermion via chiral symmetry breaking in a pure SU(2) gauge field. In the Standard Model, the masses of all elementary particles originate from the Higgs mechanism. Fermions themselves have no mass terms; they acquire mass through Yukawa coupling with the Higgs field, which simultaneously gives mass to the W and Z bosons and to the fermions [1]. Here we consider a more fundamental question: can an originally massless fermion acquire mass solely through the self-interactions of a non-Abelian gauge field?

To this end, we set the bare fermion mass $\lambda = 0$ and the mass parameter of the massless bosons $\kappa = 0$. The coupling strength $g$ is varied for comparison. To model the bosonic evolution, we employ both the Wiener process and the OU process with various mean-reversion parameters $\alpha$. At the initial time $t = 0$, all bosonic fields are set to zero (vacuum state), and the wavefunction vector $\vec{f}$ is initialized to a constant with equal components:

$$f_L(0; \vec{\varphi}_m) = f_R(0; \vec{\varphi}_m) = \frac{1}{\sqrt{2}}, \qquad (m = 1, 2, \ldots, M). \tag{8.29}$$

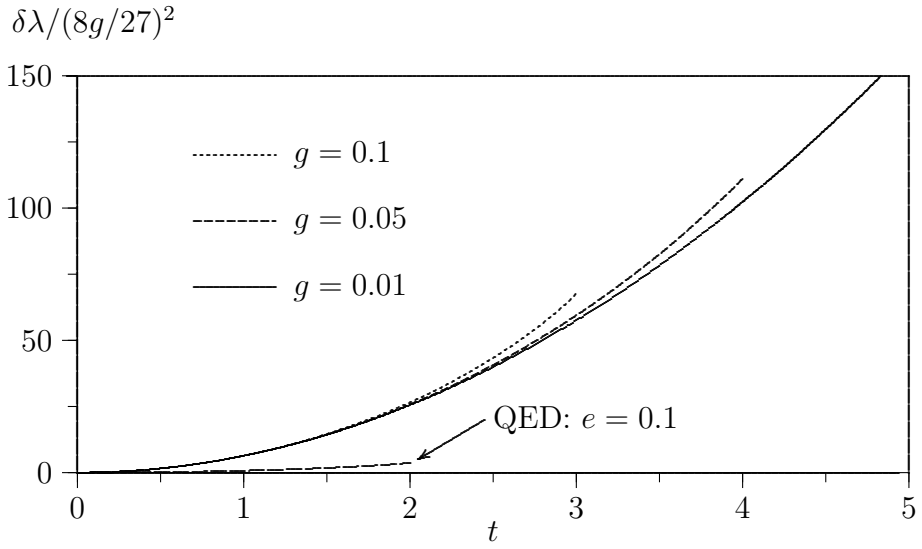


Figure 8.1: Normalized fermion mass shift $\delta\lambda\,/\,(8g/27)^2$ as a function of time $t$ in the SU(2) Yang-Mills gauge field model with a Wiener process. Parameters: $\lambda = 0$, $\kappa = 0$. Number of Monte Carlo paths: 200,000.

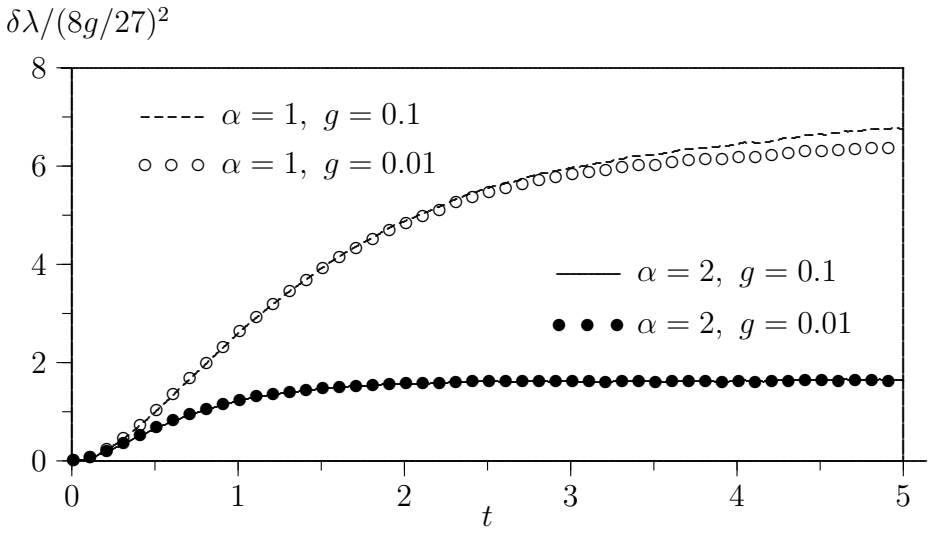


Figure 8.2: Normalized fermion mass shift $\delta\lambda\,/\,(8g/27)^2$ as a function of time $t$ in the SU(2) Yang-Mills gauge field model with a OU process. Parameters: $\lambda = 0$, $\kappa = 0$. Number of Monte Carlo paths: 200,000.

Following the procedure used in the Yukawa and QED models, we can obtain the formula for the fermion mass shift by comparing the fermionic mass term (8.11) and the interaction term (8.12) in the Lagrangian. However, in the present case, the interaction term contains an imaginary part. This may indicate that the non-Abelian gauge field model generates a dynamical imaginary mass in other directions, which is beyond the scope of this paper. Therefore, we still focus on the original Dirac fermion mass problem, restricting the mass to be real, and attribute the dynamical mass to the real part of the interaction term. The resulting dynamical mass shift is then

$$\delta\lambda = \frac{8g}{27} \frac{\sum_m \left(\varphi_1^1 + \varphi_2^2 + \varphi_3^3\right)_m (j_0)_m}{\sum_m (j_1)_m}, \tag{8.30}$$

where $m$ is the Monte Carlo path label. As mentioned earlier, among the nine bosonic components participating in the evolution, only three contribute to the dynamical fermion mass (one for each color index $a$). We also remark that for the initial condition (8.29), $f_R = f_L$ holds at every time step; thus $(j_1)_m = (j_0)_m$.

The results obtained with the Wiener process are shown in Figure 8.1. They indicate that an initially massless fermion can indeed acquire mass through self-interactions with a non-Abelian SU(2) Yang-Mills gauge field. Compared to the QED model, where only one Brownian motion drives the dynamical mass generation, the SU(2) model involves three Brownian motions, leading to a much stronger increase in the early-time dynamical mass.

Figure 8.2 shows the results obtained with the OU process. As noted earlier, the OU process describes bosonic fields that gradually return to the vacuum during evolution. The mass shift approaches a finite value after an initial increase, indicating a stable coupling between the fermionic field and the bosonic SU(2) Yang-Mills gauge field.

# 9 SU(3) Yang-Mills (QCD) with quarks

We consider the coupling of SU(3) Yang-Mills vector fields (gluons) with a quark field. The gluon field $A_\mu^a$ carries a color index $a = 1, \ldots, 8$ (adjoint representation). The quark field $\psi_c$

carries a color index $c = 1, 2, 3$ (fundamental representation). The Lagrangian is

$$\mathcal{L} = -\frac{1}{4}\big(F^a_{\mu\nu}\big)^2 + \bar{\psi}_c\big(\mathrm{i}\gamma^\mu D_\mu - \lambda\big)\psi_c, \tag{9.1}$$

where

$$F^a_{\mu\nu} = \partial_\mu A^a_\nu - \partial_\nu A^a_\mu + \hat{g} f^{abc} A^b_\mu A^c_\nu, \tag{9.2}$$

and the covariant derivative acts on the quark field as

$$(D_\mu)_{cd}\psi_d = \partial_\mu \psi_c - \mathrm{i}\hat{g}(T^a)_{cd} A^a_\mu \psi_d. \tag{9.3}$$

Here $f^{abc}$ are the SU(3) structure constants, and $T^a$ are the generators in the fundamental representation (Gell-Mann matrices normalized as $\mathrm{Tr}(T^a T^b) = \delta^{ab}/2$). The indices $c, d = 1, 2, 3$ label the quark color, while $a, b = 1, \ldots, 8$ label the gluon color. $\gamma^\mu$ ($\mu = 0, 1, 2, 3$) are the Dirac matrices, and $\lambda$ is the bare quark mass.

We adopt the radiation (Coulomb) gauge condition by setting $A^a_0 = 0$ for $a = 1, \ldots, 8$. The remaining $8 \times 3 = 24$ bosonic fields $A^a_i$ are grouped into eight vectors according to the color index $a$:

$$\vec{A}^a = (A^a_1,\ A^a_2,\ A^a_3)^T, \qquad (a = 1, \ldots, 8). \tag{9.4}$$

Then, expanding the field strength squared, the Lagrangian in (9.1) can be written explicitly as

$$\begin{aligned}
\mathcal{L} = {} & \frac{1}{2}\sum_{a=1}^{8} |\dot{\vec{A}}^a|^2 - \frac{1}{2}\sum_{a=1}^{8} |\nabla \times \vec{A}^a|^2 - \hat{g}\sum_{a,b,c=1}^{8}\sum_{i<j} f^{abc}(\partial_i A^a_j - \partial_j A^a_i) A^b_i A^c_j \\
& - \frac{\hat{g}^2}{4}\sum_{a,b,c,d,e=1}^{8} f^{abc} f^{ade} (\vec{A}^b \cdot \vec{A}^c)(\vec{A}^d \cdot \vec{A}^e) \\
& + \sum_{c=1}^{3} \bar{\psi}_c\big(\mathrm{i}\gamma^0\partial_0 + \mathrm{i}\vec{\gamma}\cdot\nabla - \lambda\big)\psi_c + \hat{g}\sum_{a=1}^{8}\sum_{i=1}^{3}\sum_{c,d=1}^{3} \bar{\psi}_c\big(\gamma^i T^a_{cd} A^a_i\big)\psi_d.
\end{aligned} \tag{9.5}$$

Here, the summations over spatial indices $i, j = 1, 2, 3$ are explicitly shown, and $i < j$ runs over the three spatial directions.

We continue to take the localized excitation assumption, decompose the gauge field $\vec{A}^a$ into a product of a spatial shape function and a time-dependent amplitude:

$$\vec{A}^a(t, \vec{x}) = F(\vec{x})\,\vec{\varphi}^a(t), \qquad (a = 1, \ldots, 8), \tag{9.6}$$

where $\vec{\varphi}^a = (\varphi_1^a, \varphi_2^a, \varphi_3^a)^T \in \mathbb{R}^3$ is a function of time $t$, and $F(\vec{x})$ is a normalized, spherically symmetric spatial distribution function centered at the origin:

$$F(\vec{x}) = \sqrt{\frac{\kappa^3}{\pi}}\, e^{-\kappa r}, \qquad r = |\vec{x}|. \tag{9.7}$$

Taking the spatial integral of the gauge-field part of the Lagrangian density (9.5), the $A^3$ term vanishes because the terms involving $\partial_i A_j^a$ are odd in the spatial coordinates. Then we have

$$T_{\text{gauge}}(t) = \int_{\mathbb{R}^3} \mathrm{d}^3x\, \frac{1}{2} \sum_{a=1}^{8} \left|\dot{\vec{A}}^a\right|^2 = \frac{1}{2} \sum_{a=1}^{8} |\dot{\vec{\varphi}}^a|^2, \tag{9.8}$$

$$\begin{aligned} V_{\text{gauge}}(t) &= \int_{\mathbb{R}^3} \mathrm{d}^3x\, \frac{1}{2} \sum_{a=1}^{8} \left|\nabla \times \vec{A}^a\right|^2 + \int_{\mathbb{R}^3} \mathrm{d}^3x\, \frac{\hat{g}^2}{4} \sum_{a,b,c,d=1}^{8} f^{abc} f^{ade} (\vec{A}^b \cdot \vec{A}^c)(\vec{A}^d \cdot \vec{A}^e) \\ &= \frac{\kappa^2}{3} \sum_{a=1}^{8} |\vec{\varphi}^a|^2 + \frac{g^2}{32} \sum_{a,b,c,d=1}^{8} f^{abc} f^{ade} (\vec{\varphi}^b \cdot \vec{\varphi}^c)(\vec{\varphi}^d \cdot \vec{\varphi}^e), \end{aligned} \tag{9.9}$$

where we have introduced the effective coupling constant $g = \sqrt{\kappa^3/\pi}\, \hat{g}$ to simplify the notation. The quadratic term coefficient $\kappa^2/3$ is obtained from the spatial integral of $|\nabla \times \vec{A}^a|^2$ using the same calculation as in the SU(2) case, which is independent of the color index $a$. The quartic term retains the full SU(3) structure. The constants $f^{abc}$ are fully antisymmetric. Their non-zero independent components (with $a < b < c$) are

$$\begin{aligned} &f^{123} = 1, \quad f^{458} = f^{678} = \frac{\sqrt{3}}{2}, \\ &f^{147} = -f^{156} = f^{246} = f^{257} = f^{345} = -f^{367} = \frac{1}{2} \end{aligned} \tag{9.10}$$

with all other components determined by antisymmetry. In numerical simulations, we first check whether $f^{abc}$ and $f^{ade}$ are non-zero; only when both are non-zero do we compute the associated inner products $(\vec{\varphi}^b \cdot \vec{\varphi}^c)$ and $(\vec{\varphi}^d \cdot \vec{\varphi}^e)$, thereby reducing computational cost.

To focus on the coupling of the quark field $\psi_c$ with the gluon fields, we note that $\psi_c$ carries a color index $c = 1, 2, 3$ and a spinor index. In the chiral representation, we decompose the quark field into left-handed and right-handed Weyl fields for each color:

$$\psi_c = \begin{pmatrix} \psi_{Lc} \\ \psi_{Rc} \end{pmatrix}, \qquad c = 1, 2, 3. \tag{9.11}$$

We also assume a localized spatial excitation, reducing the Weyl fields to a product of a spatial shape function and time-dependent complex amplitudes:

$$\psi_{Lc}(t,\vec{x}) = F(\vec{x})\, q_{Lc}(t), \qquad \psi_{Rc}(t,\vec{x}) = F(\vec{x})\, q_{Rc}(t), \tag{9.12}$$

where $F(\vec{x})$ is the same spherically symmetric function as in (9.7). For numerical implementation, we arrange the 6-component amplitude vector in the order of color outer index and chiral inner index:

$$\vec{q}(t) = \big(q_{L1},\ q_{R1},\ q_{L2},\ q_{R2},\ q_{L3},\ q_{R3}\big)^T \in \mathbb{C}^6. \tag{9.13}$$

Thus, each color $c$ corresponds to a two-dimensional subspace $(q_{Lc}, q_{Rc})^T$.

Performing the spatial integration for the fermionic part of the Lagrangian density (9.5), and noting that the term involving $\nabla\psi$ is odd in the spatial coordinates and thus integrates to zero, we obtain

$$\begin{aligned} L_{\text{fermi}}(t) &= \int_{\mathbb{R}^3} \mathrm{d}^3x \ \sum_{c=1}^{3} \bar{\psi}_c\big(\mathrm{i}\gamma^0\partial_0 + \mathrm{i}\vec{\gamma}\cdot\nabla - \lambda\big)\psi_c \\ &= \mathrm{i}\sum_{c=1}^{3}\big(q_{Lc}^*\dot{q}_{Lc} + q_{Rc}^*\dot{q}_{Rc}\big) - \lambda\sum_{c=1}^{3}\big(q_{Lc}^* q_{Rc} + q_{Rc}^* q_{Lc}\big) \\ &= \mathrm{i}\vec{q}^{\,\dagger}\dot{\vec{q}} - \lambda\,\vec{q}^{\,\dagger}\big(I_3\otimes\sigma_1\big)\vec{q}, \end{aligned} \tag{9.14}$$

where $(I_3\otimes\sigma_1)$ is the $6\times 6$ matrix acting in color-chiral space. In block form, with the color index as the outer index and the chiral index as the inner index, it is given by

$$I_3\otimes\sigma_1 = \begin{pmatrix} \sigma_1 & 0 & 0 \\ 0 & \sigma_1 & 0 \\ 0 & 0 & \sigma_1 \end{pmatrix}, \qquad \sigma_1 = \begin{pmatrix} 0 & 1 \\ 1 & 0 \end{pmatrix}. \tag{9.15}$$

Thus, the bare mass term $\lambda$ couples left- and right-handed components of the same color, as expected.

For the interaction term, following the same procedure as in the SU(2) case, we obtain

$$\begin{aligned} L_{\text{int}}(t) &= \int_{\mathbb{R}^3} \mathrm{d}^3x\ \hat{g} \sum_{a=1}^{8}\sum_{i=1}^{3}\sum_{c,d=1}^{3} \bar{\psi}_c\big(\gamma^i T^a_{cd} A^a_i\big)\psi_d \\ &= \hat{g}\bigg(\int_{\mathbb{R}^3} F^3(\vec{x})\,\mathrm{d}^3x\bigg) \sum_{a=1}^{8}\sum_{i=1}^{3}\sum_{c,d=1}^{3} q^\dagger_c\big(\sigma_i\, T^a_{cd}\,\varphi^a_i\big) q_d \\ &= \frac{8}{27} g \sum_{a=1}^{8}\sum_{i=1}^{3} \varphi^a_i\, \vec{q}^{\,\dagger}\big(T^a \otimes \sigma_i\big)\vec{q}, \end{aligned} \tag{9.16}$$

where $g = \sqrt{\kappa^3/\pi}\,\hat{g}$. In the same block form, $\big(T^a \otimes \sigma_i\big)$ is expressed as

$$T^a \otimes \sigma_i = \begin{pmatrix} T^a_{11}\sigma_i & T^a_{12}\sigma_i & T^a_{13}\sigma_i \\ T^a_{21}\sigma_i & T^a_{22}\sigma_i & T^a_{23}\sigma_i \\ T^a_{31}\sigma_i & T^a_{32}\sigma_i & T^a_{33}\sigma_i \end{pmatrix}, \tag{9.17}$$

where each $T^a_{cd}\,\sigma_i$ is a $2\times 2$ matrix acting on the chiral indices of the $(c,d)$ color pair. This block form is structurally identical to that of $(I_3\otimes\sigma_1)$ in (9.15), ensuring a uniform treatment of color and chiral degrees of freedom. In the above expressions, the eight SU(3) generators in the fundamental representation are given by

$$\begin{aligned} T^1 &= \frac{1}{2}\begin{pmatrix} 0 & 1 & 0 \\ 1 & 0 & 0 \\ 0 & 0 & 0 \end{pmatrix}, \qquad T^2 = \frac{1}{2}\begin{pmatrix} 0 & -\mathrm{i} & 0 \\ \mathrm{i} & 0 & 0 \\ 0 & 0 & 0 \end{pmatrix}, \qquad T^3 = \frac{1}{2}\begin{pmatrix} 1 & 0 & 0 \\ 0 & -1 & 0 \\ 0 & 0 & 0 \end{pmatrix}, \\ T^4 &= \frac{1}{2}\begin{pmatrix} 0 & 0 & 1 \\ 0 & 0 & 0 \\ 1 & 0 & 0 \end{pmatrix}, \qquad T^5 = \frac{1}{2}\begin{pmatrix} 0 & 0 & -\mathrm{i} \\ 0 & 0 & 0 \\ \mathrm{i} & 0 & 0 \end{pmatrix}, \qquad T^6 = \frac{1}{2}\begin{pmatrix} 0 & 0 & 0 \\ 0 & 0 & 1 \\ 0 & 1 & 0 \end{pmatrix}, \\ T^7 &= \frac{1}{2}\begin{pmatrix} 0 & 0 & 0 \\ 0 & 0 & -\mathrm{i} \\ 0 & \mathrm{i} & 0 \end{pmatrix}, \qquad T^8 = \frac{1}{2\sqrt{3}}\begin{pmatrix} 1 & 0 & 0 \\ 0 & 1 & 0 \\ 0 & 0 & -2 \end{pmatrix}. \end{aligned} \tag{9.18}$$

These matrices satisfy the commutation relations $[T^a, T^b] = \mathrm{i} f^{abc} T^c$, where $f^{abc}$ are the SU(3) structure constants. As an example, the calculation for $a = 2$ and $i = 1$ is as follows:

$$T^2 \otimes \sigma_1 = \frac{1}{2}\begin{pmatrix} 0 & -\mathrm{i}\sigma_1 & 0 \\ \mathrm{i}\sigma_1 & 0 & 0 \\ 0 & 0 & 0 \end{pmatrix} = \frac{1}{2}\begin{pmatrix} 0 & 0 & 0 & -\mathrm{i} & 0 & 0 \\ 0 & 0 & -\mathrm{i} & 0 & 0 & 0 \\ 0 & \mathrm{i} & 0 & 0 & 0 & 0 \\ \mathrm{i} & 0 & 0 & 0 & 0 & 0 \\ 0 & 0 & 0 & 0 & 0 & 0 \\ 0 & 0 & 0 & 0 & 0 & 0 \end{pmatrix}. \tag{9.19}$$

For numerical implementation, it is convenient to precompute all $8\times3 = 24$ matrices $(T^a\otimes\sigma_i)$ as $6 \times 6$ arrays, which can be used to compute $\vec{q}^{\dagger}\big(T^a \otimes \sigma_i\big)\vec{q}$ repeatedly in every time step.

Combining the expressions for the gauge kinetic term (9.8), the gauge potential term (9.9), the fermionic term (9.14), and the interaction term (9.16), we obtain the effective action for the SU(3) Yang-Mills QCD model within the stochastic framework:

$$S(T) = \int \mathrm{d}^4x\, \mathcal{L} = \int_0^T \mathrm{d}t \left(T_{\text{gauge}}(t) - V_{\text{gauge}}(t) + L_{\text{fermi}}(t) + L_{\text{int}}(t)\right). \tag{9.20}$$

This action describes a finite-dimensional system of coupled bosonic variables $\vec{\varphi}^a(t) \in \mathbb{R}^3$ ($a = 1, \cdots, 8$, one for each color generator) and fermionic variables $\vec{q}(t) \in \mathbb{C}^6$. The bosonic part retains the characteristic nonlinear self-interaction of SU(3) Yang-Mills theory, while the fermionic part exhibits a gauge-induced mass mixing. This formulation is well-suited for stochastic quantization and can be solved numerically using Monte Carlo methods.

Now we derive the numerical scheme for the coupled evolution of the SU(3) Yang-Mills gauge field and the Dirac fermion. We define a wavefunction vector that depends on the bosonic configuration:

$$\vec{f}(t;\vec{\varphi}) = \begin{pmatrix} f_{L1}(t;\vec{\varphi}) \\ f_{R1}(t;\vec{\varphi}) \\ f_{L2}(t;\vec{\varphi}) \\ f_{R2}(t;\vec{\varphi}) \\ f_{L3}(t;\vec{\varphi}) \\ f_{R3}(t;\vec{\varphi}) \end{pmatrix}, \tag{9.21}$$

where the six components are functions of $\vec{\varphi} = (\vec{\varphi}^1, \vec{\varphi}^2, \ldots, \vec{\varphi}^8)^T$, the SU(3) gauge field configuration with each $\vec{\varphi}^a \in \mathbb{R}^3$. These components evolve according to the Wiener process (or Ornstein-Uhlenbeck process) governing the bosonic fields. The three components $f_{L1}, f_{L2}, f_{L3}$ correspond to the left-handed components of the three color states, while $f_{R1}, f_{R2}, f_{R3}$ correspond to the right-handed components. Their dynamics is described by a Poisson jump process with intensity $\lambda$.

For numerical implementation of the evolution of $\vec{f}$, we discretize time $t \geq 0$ into intervals of equal length $\Delta t$, denoted by $[t^n, t^{n+1}]$. At each time step $t^n$, the continuous bosonic field $\vec{\varphi}$ is discretized into $M$ independent states (or paths) $\vec{\varphi}_m$ $(m = 1, 2, \ldots, M)$. Thus, at each time $t^n$ we have $M$ independent samples of the wavefunction vector:

$$\vec{f}(t^n, \vec{\varphi}_m), \qquad (m = 1, 2, \ldots, M). \tag{9.22}$$

In the time direction, we employ a first-order operator splitting scheme to update $\vec{f}$ over $[t^n, t^{n+1}]$ in two steps. The first step updates $\vec{f}$ according to the bosonic evolution rule:

$$\vec{f}(t^{n+1/2}; \vec{\varphi}_m^{n+1}) = \mathbb{K}^{\vec{\varphi}}\Big[\vec{f}(t^n; \vec{\varphi}_m^n)\Big], \tag{9.23}$$

and the second step updates $\vec{f}$ according to the fermionic evolution rule:

$$\vec{f}(t^{n+1}; \vec{\varphi}_m^{n+1}) = \mathbb{K}^{\vec{q}}\Big[\vec{f}(t^{n+1/2}; \vec{\varphi}_m^{n+1})\Big]. \tag{9.24}$$

We first derive the explicit form of the first evolution operator $\mathbb{K}^{\vec{\varphi}}$. In the stochastic formulation, all six components $f_{Lc}$ and $f_{Rc}$ ($c = 1, 2, 3$) of the fermion wavefunction are driven by the eight bosonic vectors $\vec{\varphi}^a$ ($a = 1, \ldots, 8$), corresponding to a total of $8 \times 3 = 24$ independent components. The evolution of these bosonic vectors can be simulated by 24 mutually independent Brownian motions. In numerical simulations, each Brownian motion is represented by a one-dimensional array, and we will adopt the Monte Carlo method for computation.

In the simulation, we first apply the transformation $\vec{\varphi}^a = \sqrt{\mathrm{i}}\,\vec{u}^a$ to the Lagrangian, so that each $\vec{u}^a$ follows a three-dimensional Ornstein-Uhlenbeck process. On each Monte Carlo path $m$, time is discretized with step size $\Delta t$, and the process is simulated using Gaussian random numbers:

$$\vec{u}_m^a(t^{n+1}) = (1 - \alpha\Delta t)\,\vec{u}_m^a(t^n) + \sigma\sqrt{\Delta t}\,\vec{\xi}_m^a, \qquad \vec{\xi}_m^a \sim \mathcal{N}(0, I_3), \tag{9.25}$$

where the volatility parameter is set to $\sigma = 1$, and the mean-reversion parameter $\alpha$ is to be determined. This gives the "coordinates" for $\vec{f}(t^{n+1}; \vec{\varphi}_m^{n+1})$ at the next time step.

According to the stochastic formulation, the bosonic evolution for the wave function $\vec{f}(t; \vec{\varphi})$ is given by

$$\vec{f}(t^{n+1/2}; \vec{\varphi}^{n+1}) = \exp\Big(A + B + C\Big)\,\vec{f}(t^n; \vec{\varphi}^n), \tag{9.26}$$

where $\vec{f}(t^n;\vec{\varphi}^n)$ is the wave function at the current time step, and

$$A = \frac{\kappa^2}{3}\Delta t \sum_{a=1}^{8} |\vec{u}^a|^2, \tag{9.27}$$

$$B = \mathrm{i}\frac{g^2}{32}\Delta t \sum_{a,b,c,d,e=1}^{8} f^{abc} f^{ade} (\vec{u}^b \cdot \vec{u}^c)(\vec{u}^d \cdot \vec{u}^e), \tag{9.28}$$

$$C = \mathrm{i}^{3/2}\frac{8}{27} g\Delta t \sum_{a=1}^{8}\sum_{i=1}^{3} u_i^a \, j_i^a, \tag{9.29}$$

with the color-chiral currents defined as

$$j_i^a = \vec{f}^{\dagger}(T^a \otimes \sigma_i)\vec{f}, \tag{9.30}$$

which is precomputed with the $6\times 6$ matrices $T^a \otimes \sigma_i$ at previous time step. Unlike in SU(2) model, the currents $j_i^a$ will be kept as complex number in computation.

We now derive the second evolution operator $\mathbb{K}^{\vec{q}}$. Based on (9.14) and (9.16), the Euler-Lagrange equation for the fermionic wave vector $\vec{f}(t;\vec{\varphi})$ is

$$\mathrm{i}\dot{\vec{f}} = H\,\vec{f}, \tag{9.31}$$

where the $6 \times 6$ effective Hamiltonian is constructed from the bosonic configuration $\vec{\varphi}^n$:

$$H(\vec{\varphi}^n) = \lambda\,(I_3 \otimes \sigma_1) + \frac{8}{27} g \sum_{a=1}^{8}\sum_{i=1}^{3} \varphi_i^a\,(T^a \otimes \sigma_i). \tag{9.32}$$

The evolution equation for $\vec{f}$ is then

$$\vec{f}(t^{n+1};\vec{\varphi}^{n+1}) = e^{-\mathrm{i}H\Delta t}\,\vec{f}(t^{n+1/2};\vec{\varphi}^{n+1}). \tag{9.33}$$

In practice, at each time step and for each configuration $\vec{\varphi}_m$, we construct the $6\times 6$ matrix $H$ and compute its matrix exponential. Since $\Delta t$ is small, we can use a Taylor series expansion:

$$e^{-\mathrm{i}H\Delta t} \approx I_6 - \mathrm{i}H\Delta t - \frac{1}{2}H^2\Delta t^2 + \mathcal{O}(\Delta t^3). \tag{9.34}$$

Then, using (9.33), we obtain $\vec{f}(t^{n+1};\vec{\varphi}^{n+1})$, completing all computations for this $\Delta t$ cycle.

The fermionic evolution in this SU(3) model is very similar in structure to that of the SU(2) model, but it is driven by 24 bosonic components, which makes it more prone to

dynamical chiral symmetry breaking. This reflects the richer dynamics inherent in non-Abelian gauge fields. We now discuss how to compute the fermion mass shift from the evolved wavefunction. Instead of relying on a specific analytic projection, we extract the dynamical mass directly from the effective fermionic current. Comparing the fermionic Lagrangian (9.14) and interaction Lagrangian (9.16), we know on each path $m$, the instantaneous current is

$$-\lambda\, \vec{f}_m^{\dagger}(I_3 \otimes \sigma_1)\vec{f}_m + \frac{8}{27} g \sum_{a=1}^{8}\sum_{i=1}^{3} \varphi_i^a\, \vec{f}_m^{\dagger}(T^a \otimes \sigma_i)\vec{f}_m. \tag{9.35}$$

The dynamical fermion mass is then obtained from the expectation value of the scalar part of the interaction, taking its real part:

$$\delta\lambda = \mathrm{Re}\left( \frac{8}{27} g \frac{\sum_m \vec{f}_m^{\dagger}\Big(\sum_{a=1}^{8}\sum_{i=1}^{3} \varphi_i^a\,(T^a \otimes \sigma_i)\Big)\vec{f}_m}{\sum_m \vec{f}_m^{\dagger}(I_3 \otimes \sigma_1)\vec{f}_m} \right). \tag{9.36}$$

This expression reduces to the SU(2) formula when the color indices are truncated, but for SU(3) it serves as a numerical definition that automatically accounts for all contributions, with the real part taken to ensure a physical result.

As the initial condition, at time $t = 0$ all bosonic fields are set to zero (vacuum state), and the wavefunction vector $\vec{f}$ is initialized as

$$\vec{f}(0;\vec{\varphi}_m) = \frac{1}{\sqrt{6}}(1,1,1,1,1,1)^T, \qquad (m = 1,2,\ldots,M). \tag{9.37}$$

This choice guarantees each fermion component have an equal weight at evolution start, ensuring an observation on their symmetric features.

Figure 9.1 shows the results obtained with the Wiener process for three different values of the coupling parameter $g$. They confirm that the system of three initially massless fermions in the QCD model can acquire mass through self-interactions with a non-Abelian SU(3) Yang-Mills gauge field. This phenomenon is the direct analogue of dynamical chiral symmetry breaking in QCD, where the quark condensate $\langle\bar{q}q\rangle \neq 0$ has been firmly established by experiment through the Gell-Mann–Oakes–Renner relation [12] and confirmed by QCD sum rules [13] as well as lattice QCD calculations [14].

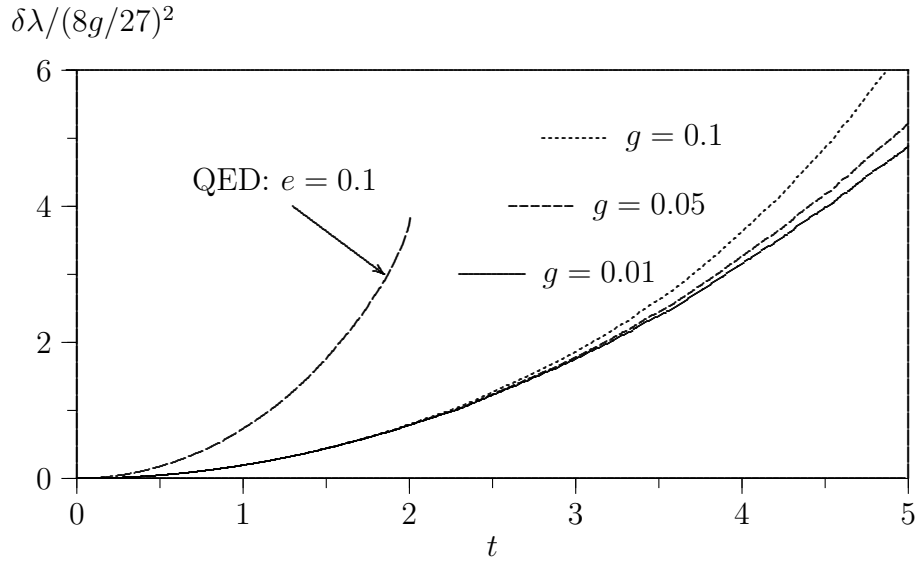


Figure 9.1: Normalized fermion mass shift $\delta\lambda/(8g/27)^2$ as a function of time $t$ in the SU(3) QCD model with a Wiener process. Parameters: $\lambda = 0$, $\kappa = 0$. Number of Monte Carlo paths: 200,000.

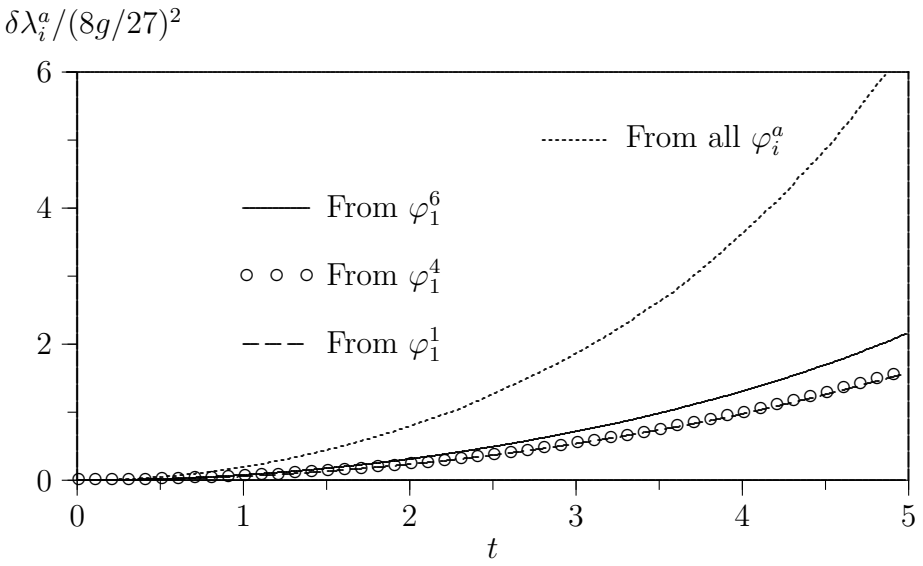


Figure 9.2: Normalized fermion mass shift $\delta\lambda/(8g/27)^2$ from the three major components $\varphi_i^a$ as a function of time $t$ in the SU(3) QCD model with a Wiener process. Parameters: $\lambda = 0$, $\kappa = 0$, $g = 0.1$. Number of Monte Carlo paths: 200,000.

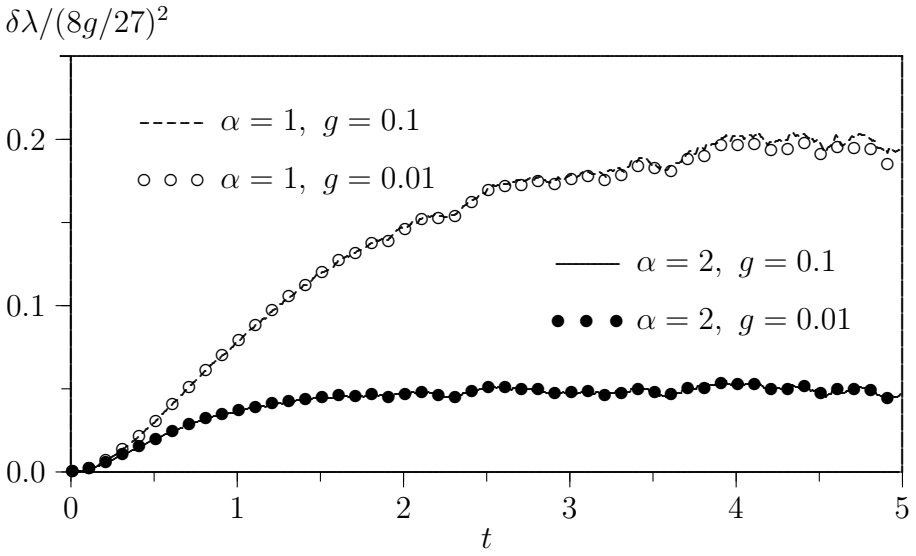


Figure 9.3: Normalized fermion mass shift $\delta\lambda/(8g/27)^2$ as a function of time $t$ in the SU(3) QCD model with an OU process. Parameters: $\lambda = 0$, $\kappa = 0$. Number of Monte Carlo paths: 200,000.

A notable feature in Figure 9.1 is that the magnitude of the mass shift is significantly smaller than in the SU(2) and QED models, despite the SU(3) system involving 24 bosonic components. To explain this phenomenon, we decompose the total mass shift (9.36) into contributions from the 24 individual bosonic components $\varphi_i^a$ as

$$\delta\lambda_i^a = \mathrm{Re}\left(\frac{8}{27}g\,\frac{\sum_m \vec{f}_m^{\dagger}\left(\varphi_i^a\,(T^a\otimes\sigma_i)\right)\vec{f}_m}{\sum_m \vec{f}_m^{\dagger}(I_3\otimes\sigma_1)\vec{f}_m}\right). \tag{9.38}$$

As shown in Figure 9.2, the total dynamical mass in the SU(3) model is predominantly generated by three bosonic components: $\varphi_1^1$, $\varphi_1^4$, and $\varphi_1^6$, which together account for about 83% of the total mass contribution. The remaining components contribute at a much smaller level. Unlike in the QED and SU(2) models, where only the two chiral components of a single fermion are involved in the coupling, the three dominant bosons in the SU(3) model correspond to the off-diagonal color generators $T^1$, $T^4$, and $T^6$, which drive couplings between fermions of different colors.

Figure 9.2 also shows that the mass shift contributions from the three dominant bosons are not equal; their ratio is approximately $1:1:1.4$, indicating a departure from exact color symmetry. The color structure of SU(3) provides a natural explanation for this observation.

From (9.18), the generators $T^1$ and $T^2$ mix colors 1 and 2; $T^4$ and $T^5$ mix colors 1 and 3; and $T^6$ and $T^7$ mix colors 2 and 3. The diagonal generators $T^3$ and $T^8$ couple each color to itself, but with unequal coefficients:

$$T^3 = \frac{1}{2}\,\mathrm{diag}(1,-1,0), \qquad T^8 = \frac{1}{2\sqrt{3}}\,\mathrm{diag}(1,1,-2).$$

Summing the diagonal coefficients yields $1/2 + 1/(2\sqrt{3}) = 0.7887$ for color 1, $-0.2113$ for color 2, and $-0.5774$ for color 3. Thus, color 1 is distinguished from colors 2 and 3, while colors 2 and 3 have similar (both negative) coefficients. This asymmetry naturally leads to unequal mass contributions from the three color-pair channels: the 1–2 and 1–3 channels contribute similarly, while the 2–3 channel contributes differently. This is precisely reflected in the numerical ratio $\varphi_1^1 : \varphi_1^4 : \varphi_1^6 \approx 1 : 1 : 1.4$.

As in the SU(2) and other models, the Ornstein-Uhlenbeck process describes bosonic fields that gradually return to the vacuum during evolution in the SU(3) QCD model. Figure 9.3 shows the results obtained with the OU process. The mass shift approaches a finite value after an initial increase, indicating a stable coupling between the fermionic field and the bosonic SU(3) QCD gauge field. This behavior mirrors the physical picture of QCD, where quarks acquire the bulk of their mass dynamically through interactions with the gluon field, while their bare masses are small. In contrast, the Wiener process ($\alpha = 0$) leads to unbounded mass growth, which is non-physical. The mean-reversion parameter $\alpha$ thus controls the relaxation scale of the bosonic field, and its proper choice allows the model to reproduce the observed dynamical mass scale, consistent with lattice QCD and phenomenological determinations of the quark condensate.

# 10 Conclusion

In summary, this work presents a rigorous framework for formulating and computing real-time quantum field dynamics. By establishing a precise correspondence between quantum fields and classical stochastic processes, we have shown that the complex phase interference inherent in the Feynman path integral can be exactly mapped onto the probabilistic evolution of Wiener and Poisson processes.

Our applications to the Yukawa and QED models validate this formalism, revealing non-trivial dynamical features such as the independence of dynamical fermion mass generation from the initial fermion mass. The introduction of an Ornstein-Uhlenbeck (OU) process provides stable evolution with controlled relaxation toward the vacuum, enabling long-time extraction of finite physical observables, such as the dynamical fermion mass.

The extension to non-Abelian gauge theories further demonstrates the power of the framework. In pure SU(2) Yang-Mills theory coupled to a Dirac fermion, we observe dynamical fermion mass generation in the chiral limit, driven purely by specific bosonic components in the gauge field self-interactions. This mechanism naturally generalizes to SU(3) QCD, where the color structure induces a non-zero mass shift through chiral symmetry breaking, consistent with experimental results and lattice QCD calculations.

The present work has established a robust stochastic framework for real-time dynamics within the localized excitation approximation, successfully capturing non-perturbative phenomena such as dynamical mass generation. An immediate and natural extension is to relax this approximation by reintroducing spatial degrees of freedom on a lattice. This will enable the direct computation of spatially extended observables, including Wilson loops for the confining potential and two-point correlation functions for the hadron spectrum (mesons, baryons, and glueballs). Such an extension would elevate our stochastic formulation to a comprehensive, first-principles tool for investigating the full landscape of QCD, bridging the gap between real-time dynamics and the static properties probed by conventional Euclidean lattice methods.

**Acknowledgement:** The author gratefully acknowledges Professor James Glimm from Stony Brook University. His introduction to the Feynman-Kac formalism motivated this research, and his insightful discussions on fermions and strong coupling problems were instrumental to the success of this paper. The author acknowledges the support of the Alexander von Humboldt Foundation.

# 11 Appendix

In this appendix we re-derive the classical analytic expression for the transition amplitude of a one-dimensional harmonic oscillator under a constant external source. Let the state function of the oscillator be $\varphi(t)$ with the Lagrangian action

$$\mathcal{L} = S[\varphi(t)] = \int \mathrm{d}t \Big[\frac{1}{2}\dot{\varphi}^2 - \frac{1}{2}\omega^2\varphi^2 + J_0\varphi\Big]. \tag{11.1}$$

We wish to compute the transition amplitude for the particle to go from an initial state $\varphi(0) = a$ to a final state $\varphi(T) = b$ via all possible paths:

$$K(b, T; a, 0) = \int_{\varphi(0)=a}^{\varphi(T)=b} \mathcal{D}\varphi \; e^{\mathrm{i}S[\varphi]}. \tag{11.2}$$

Following Feynman's approach [5], we decompose $\varphi(t)$ into a classical solution $x_c(t)$ and a fluctuation part $y(t)$:

$$\varphi(t) = x_c(t) + y(t), \tag{11.3}$$

where the classical solution $x_c(t)$ satisfies the driven equation of motion

$$\ddot{x}_c + \omega^2 x_c = J_0, \tag{11.4}$$

together with the boundary conditions $x_c(0) = a$, $x_c(T) = b$. The fluctuation $y(t)$ obeys zero boundary conditions, $y(0) = y(T) = 0$. The action then splits into three pieces:

$$S[\varphi(t)] = S[x_c(t)] + S[y(t)] + S_{xy}. \tag{11.5}$$

The cross term $S_{xy}$ vanishes due to the zero boundary conditions of $y$ and the fact that $x_c$ satisfies (11.4):

$$S_{xy} = \int_0^T \big(\dot{x}_c\dot{y} - \omega^2 x_c y + J_0 y\big)\mathrm{d}t = \Big[\dot{x}_c(t)y(t)\Big]\Big|_0^T + \int_0^T \big(-\ddot{x}_c - \omega^2 x_c + J_0\big)y\,\mathrm{d}t = 0.$$

The second term is the action of the homogeneous harmonic oscillator (containing no source term):

$$S[y(t)] = \int \mathrm{d}t \Big[\frac{1}{2}\dot{y}^2 - \frac{1}{2}\omega^2 y^2\Big].$$

The first term is the action of the classical solution:

$$S[x_c(t)] = \int \mathrm{d}t \Big[\frac{1}{2}\dot{x}_c^2 - \frac{1}{2}\omega^2 x_c^2 + J_0 x_c\Big],$$

which is a constant with respect to the path integral and can be taken outside. Hence,

$$K(b,T;a,0) = e^{\mathrm{i}S[x_c(t)]} \int_{y(0)=0}^{y(T)=0} \mathcal{D}y \; e^{\mathrm{i}S[y]}. \tag{11.6}$$

The remaining path integral is the propagator of a free harmonic oscillator from 0 to 0, whose analytic form is known [5]:

$$K(b,T;a,0) = \sqrt{\frac{\omega}{2\pi\mathrm{i}\,\sin(\omega T)}}\; e^{\mathrm{i}S[x_c(t)]}. \tag{11.7}$$

Thus, the problem reduces to computing the classical action $S[x_c(t)]$.

According to the equation of motion (11.4), the classical solution can be written as

$$x_c(t) = A\cos(\omega t) + B\sin(\omega t) + \frac{J_0}{\omega^2}. \tag{11.8}$$

Using the boundary conditions $x_c(0) = a$ and $x_c(T) = b$, we obtain

$$\begin{aligned} A &= a - j, \\ B &= \frac{1}{\sin\theta}\Big[(b-j) - (a-j)\cos\theta\Big], \end{aligned} \tag{11.9}$$

where, for convenience, we have introduced the abbreviations

$$j = \frac{J_0}{\omega^2}, \qquad \theta = \omega T.$$

We now proceed to evaluate the action. For a solution $x_c(t)$ satisfying the equation of motion,

$$\frac{\mathrm{d}}{\mathrm{d}t}(\dot{x}_c x_c) = \dot{x}_c^2 + x_c\ddot{x}_c = \dot{x}_c^2 - \omega^2 x_c^2 + J_0 x_c.$$

Therefore,

$$S[x_c(t)] = \int_0^T \Big[\frac{1}{2}\big(\dot{x}_c^2 - \omega^2 x_c^2\big) + J_0 x_c\Big]\mathrm{d}t = \frac{1}{2}\int_0^T \frac{\mathrm{d}}{\mathrm{d}t}(\dot{x}_c x_c)\,\mathrm{d}t + \frac{1}{2}J_0\int_0^T x_c(t)\,\mathrm{d}t.$$

The first term gives

$$\begin{aligned}
\frac{1}{2}\int_0^T \frac{\mathrm{d}}{\mathrm{d}t}(\dot{x}_c x_c)\,\mathrm{d}t &= \frac{1}{2}\Big[\dot{x}_c(T)b - \dot{x}_c(0)a\Big] \\
&= \frac{1}{2}\Big[-A\omega\sin\theta + B\omega\cos\theta\Big]b - \frac{1}{2}B\omega a \\
&= -\frac{(a-j)}{2}\omega b\sin\theta + \frac{(b-j)-(a-j)\cos\theta}{2\sin\theta}\,\omega\,(b\cos\theta - a) \\
&= \frac{\omega}{2\sin\theta}\Big[-ab\sin^2\theta + (b\cos\theta - a)(b - a\cos\theta)\Big] \\
&\qquad + \frac{j\omega}{2\sin\theta}\Big[b\sin^2\theta - (1-\cos\theta)(b\cos\theta - a)\Big] \\
&= \frac{\omega}{2\sin\theta}\Big[(a^2+b^2)\cos\theta - 2ab\Big] + \frac{j\omega}{2\sin\theta}(a+b)(1-\cos\theta).
\end{aligned}$$

The second term is

$$\begin{aligned}
\frac{J_0}{2}\int_0^T x_c(t)\,\mathrm{d}t &= \frac{J_0}{2}\int_0^T \Big[A\cos(\omega t) + B\sin(\omega t) + j\Big]\mathrm{d}t \\
&= \frac{J_0}{2\omega}\Big[A\sin\theta + B(1-\cos\theta) + j\theta\Big] \\
&= \frac{J_0}{2\omega}\Big[(a-j)\sin\theta + \frac{1}{\sin\theta}\big(b - j - (a-j)\cos\theta\big)(1-\cos\theta) + j\theta\Big] \\
&= \frac{J_0}{2\omega\sin\theta}\Big[a\sin^2\theta + (b - a\cos\theta)(1-\cos\theta)\Big] \\
&\qquad + \frac{J_0 j}{2\omega\sin\theta}\Big[-\sin^2\theta - (1-\cos\theta)^2 + \theta\sin\theta\Big] \\
&= \frac{J_0}{2\omega\sin\theta}(a+b)(1-\cos\theta) + \frac{J_0 j}{2\omega\sin\theta}\Big[\theta\sin\theta - 2(1-\cos\theta)\Big].
\end{aligned}$$

Adding the two terms and substituting $j = J_0/\omega^2$ and $\theta = \omega T$ yields

$$\begin{aligned}
S[x_c(t)] &= \frac{\omega}{2\sin(\omega T)}\Big[(a^2+b^2)\cos(\omega T) - 2ab\Big] \\
&\quad + \frac{J_0}{\omega\sin(\omega T)}(a+b)\big(1-\cos(\omega T)\big) \\
&\quad + \frac{J_0^2}{2\omega^3\sin(\omega T)}\Big[\omega T\sin(\omega T) - 2\big(1-\cos(\omega T)\big)\Big]. \qquad (11.10)
\end{aligned}$$

Inserting $S[x_c(t)]$ into (11.7) gives the complete analytic expression for $K(b,T;a,0)$. In

particular, for $a = 0$ we obtain

$$K(b,T;0,0) = \sqrt{\frac{\omega}{2\pi \mathrm{i}\,\sin(\omega T)}} \cdot \exp\Bigg\{ \mathrm{i}\,\frac{b^2\omega}{2}\frac{\cos(\omega T)}{\sin(\omega T)} + \mathrm{i}\,\frac{bJ_0}{\omega}\frac{1-\cos(\omega T)}{\sin(\omega T)} + \mathrm{i}\frac{J_0^2}{2\omega^3}\Big(\omega T - 2\frac{1-\cos(\omega T)}{\sin(\omega T)}\Big)\Bigg\}. \quad (11.11)$$

# References


[1] M. E. Peskin and D. V. Schroeder, *An Introduction to Quantum Field Theory*, Westview Press, Boulder, 1995, Section 4.2.

[2] K. G. Wilson, Confinement of quarks, *Phys. Rev. D* **10**, 2445–2459 (1974).

[3] M. Troyer and U.-J. Wiese, Computational complexity and fundamental limitations to fermionic quantum Monte Carlo simulations, *Phys. Rev. Lett.* **94**, 170201 (2005).

[4] D. B. Kaplan, A method for simulating chiral fermions on the lattice, *Phys. Lett. B* **288**, 342–347 (1992).

[5] R. P. Feynman and A. R. Hibbs, *Quantum Mechanics and Path Integrals*, McGraw-Hill, New York, 1965, pp. 170–177.

[6] J. Glimm and A. Jaffe, *Quantum Physics: A Functional Integral Point of View*, 2nd ed., Springer-Verlag, New York, 1987.

[7] G. N. Ord, Stochastic quantization and path integrals, *J. Phys. A: Math. Gen.* **16**, 1869–1885 (1983).

[8] T. Jacobson and L. S. Schulman, Quantum stochastic processes: A path integral approach, *J. Phys. A: Math. Gen.* **17**, 375–388 (1984).

[9] G. Strang, Accurate partial difference methods, II nonlinear problems, *Numer. Math.* **13**, 37–46 (1964).

[10] C. J. Burden, Fermion mass generation in the (1+1)-dimensional Yukawa model, *Nucl. Phys. B* **387**, 419–446 (1992).

[11] S. A. Chin, Yukawa model in 1+1 dimensions, *Phys. Rev. D* **42**, 699–706 (1990).

[12] M. Gell-Mann, R. J. Oakes, and B. Renner, Behavior of current divergences under SU(3) × SU(3), *Phys. Rev.* **175**, 2195 (1968).

[13] M. A. Shifman, A. I. Vainshtein, and V. I. Zakharov, QCD and resonance physics. Theoretical foundations, *Nucl. Phys. B* **147**, 385–447 (1979).

[14] H. Fukaya et al. (JLQCD Collaboration), Determination of the chiral condensate from 2+1-flavor lattice QCD, *Phys. Rev. D* **83**, 074501 (2011), arXiv:1012.4052 [hep-lat].